FINAL TECHNICAL REPORT

AWARD# 120044

Title: Earthquake Hazard of the Camarillo Fold Belt: An analysis of the Unstudied Fold Belt in the Southern California hot zone

Supervising Principle Investigators: Edward Keller and Doug Burbank

Author: Duane E. DeVecchio, Earth Research Institute, 6832 Ellison Hall, University of California, Santa Barbara, CA 93106-3060; phone: 805-403-9572; e-mail: duanedevecchio@mac.com

Proposal Category: Integration and Theory
Discipline: Earthquake Geology

Funding Period: ***February 1, 2008 to January 31, 2011***

Recent Bibliography

DeVeecchio, D. E., Heermance R. V., Fuchs, M., Owen, L. A., *in review*, Climate-controlled landscape evolution in the Western Transverse Ranges, California: Insights from Quaternary geochronology of the Saugus Formation and strath terrace flights

DeVecchio, D. E., Keller, E. A., Owen, L., Fuchs, M., *in press*, Miocene to late Pleistocene structural evolution of the Camarillo fold belt: Implications for seismic hazard and fold growth in southern California, Geological Society of America, Lithosphere.

DeVeecchio, D. E., Heermance R. V, 2011, Climate-controlled landscape evolution in the Western Transverse Ranges, California: Insights from Quaternary geochronology of aggradational deposits and bedrock erosion surfaces, American Geophysical Union Annual Meeting Abstract.

DeVecchio, D. E., and Anonymous, 2009, Punctuated lateral fold and fault growth; Camarillo fold belt, Ventura County, California, Abstracts with Programs - Geological Society of America: Boulder, Geological Society of America (GSA), p. 184.

DeVecchio, D. E., Keller, E.A., Owen, L. A., Fuchs, M., 2008, The Camarillo Fold Belt: An order of magnitude younger than previously thought, Southern California Earthquake Center, Annual meeting Abstract, vol. 18, p. 82.

Research supported by the Southern California Earthquake Center a subsidiary of the National Science Foundation. The views and conclusions contained in this document are those of the authors and should not be interpreted as necessarily representing the aforementioned agencies.

ABSTRACT

The main objective of this research is to develop the chronology of geomorphic surfaces and sedimentary strata deformed within the Camarillo fold belt (CFB) in order to estimates rates of active tectonics. The research contained within this report was funded by the Southern California Earthquake Center (SCEC, award# 120044) and the USGS (award# 8HQGR0073) and is part of DeVecchio's dissertation research.

The Camarillo Fold Belt (CFB) is composed of several south-verging anticlines, which comprise the western extent of the west-trending highly segmented Simi fault zone that extends from the northern Simi Valley to the city of Camarillo. Geologic mapping, GIS-based topographic analyses, optically stimulated luminescence (OSL) and radiocarbon dating, and subsurface well logs are integrated to bracket the relative timing of deformation on active faults, to develop a chronology of deformed surfaces, and to better constrain the age of the Saugus Formation in this part of the Western Transverse Ranges. New geochronology of the Saugus Formation exposed in the study area indicates that the the upper age limit of deformed strata are an order of magnitude younger than previously thought (~20 ka vs. 200 ka), with the onset of deposition beginning sometime after ~85 ka. This chronologic revision has significant implications for the timing and rates of deformation, as well as for the seismic hazard in the study area.

Many of the Quaternary transpressional faults are reactivated Miocene high-angle (70-80°) transrotational faults. Where the age of deformed sediments is well-known, minimum vertical uplift rates on several of the active faults are ~1.5 mm/yr, which is 3-times greater than most previous estimates based on paleoseismic investigations. Discrete structural domains are characterized by west-plunging anticlines, changes in the orientation and loci of active structures, and they are bound by fault segment boundaries that are often characterized by orthogonal north-striking faults. Structural relief and the age of deformation decrease from east to west across each successive north-striking fault. We interpret these relations to suggest that westward propagation of the fold belt occurred by punctuated lateral growth of the Simi fault due to the presence of north-trending faults. This style of deformation may be common in the Western Transverse Ranges and has important implications for seismic hazard assessment.

Geochronology of geomorphic surfaces indicates that the landscape evolution in the CFB was modulated by global climate change. A regionally extensive erosion surface (45 km^2) in the study area was cut during Marine Isotope Stage 2 (MIS2; 19-24 ka). Incision from 19-12 ka resulted in deep canyons cut throughout the study area, which were back-filled following the Pleistocene Holocene transition (12- 4 ka).

TABLE OF CONTENTS

INTRODUCTION

On October 1, 1987, much of the Los Angeles area was awakened by the M_w6.0 Whittier Narrows earthquake, which occurred on a largely unrecognized thrust fault. Less than seven years later in 1994, the strongest ground motion ever instrumentally recorded in an urban area of North America was measured during the M_w6.7 Northridge earthquake that ruptured along a completely unknown blind thrust fault and resulted in 61 deaths and ~$20 billion in damage (Fig. 1). Consequently, many geological studies in the Los Angeles basin have concluded that thrust faults pose the greatest seismic hazard in Southern California and accommodate most of the geodetically observed shortening across the Los Angeles area (e.g., USGS and SCEC Scientists, 1994; Dolan et al., 1995, 1997; Shaw and Suppe, 1996). Similarly, thrust faults in the Santa Barbara piedmont and Ventura County have accommodated significant shortening over the past 100 ky and are capable of generating earthquake magnitudes from M_w6.5-7.5 (e.g., Larsen et al., 1993; Gurrola and Keller, 1999; Dolan and Rockwell, 2001).

The presence of known fold belts within metropolitan Los Angeles and in rapidly urbanizing areas to the north has resulted in numerous studies for the purpose of evaluating the potential seismic hazard (e.g., Blake, 1991a; Hauksson et al., 1995; Treiman 1997, 1998; Walls et al., 1998; Hitchcock et al., 1998; Oskin et al., 2000; Dolan et al., 2003). Yet locating faults, assessing fault continuity along strike, and determining the rate and timing of deformation on active structures is difficult because reverse faults, in this region, are typically concealed beneath younger alluvium or blind.

This study examines the Camarillo Fold Belt (CFB) in the Western Transverse Ranges, which is composed of several south-verging folds and active reverse faults that compose the western extent of the Simi fault zone. These faults pose a hazard to nearly one million people living in the cities of Ventura, Camarillo, Thousand Oaks, and Oxnard as well as those living in the Simi and Santa Clara River Valleys (Fig. 2). Although numerous consulting reports have been generated on some of the known faults, the CFB is the only remaining fold belt between the Los Angeles fold belt and the Santa Barbara fold belt that has not been studied as a unit for the purpose of evaluating the timing and rates of deformation.

Descriptions of unlithified but folded and faulted fluvial sands and silts in the CFB are omnipresent in consulting reports and paleoseismic trench logs (Blake, 1991b *and the references therein*). These deformed sediments are commonly ascribed to the Saugus Formation and are assumed to have a minimum age of 200 ka based on limited geochronology. Yet, because age data on the Saugus Formation are sparse and no geochronologic investigation has been undertaken within the CFB, the true age of these strata is unknown. This study's goals are to assess the relative timing, rates, and magnitudes of tectonic folding along the active structures, to better bracket the age limits of the Saugus Formation, and to develop the Quaternary chronology of deformed sediments within the fold belt.

This research examines the Miocene to Quaternary structural development and late Quaternary geomorphic evolution of the CFB. New geologic mapping,

stratigraphic analysis, and cross sections based on subsurface water and petroleum well logs are used to illustrate Miocene deformation on several of the active Quaternary faults. GIS-based topographic analysis of digital elevation models (DEM) and "indices of active tectonics" (see Keller and Pinter, 2002) are utilized to develop a relative deformational chronology and to assess the late Quaternary to Holocene deformational history and relative timing of tectonic uplift of active folds. Initial geochronologic results of several of the deformed upper Pleistocene to Holocene strata using optically stimulated luminescence (OSL) and radiocarbon analyses are presented. Together these data suggest the loci and lateral continuity of late Quaternary reverse faults are controlled by Miocene transrotational faults. Orthogonal north-trending faults locally limit the lateral propagation of folds and constrain deformation on the underlying faults within discrete structural domains. Folds within the Late Quaternary structural domains in the CFB and within discrete fold complexes appear to young to the west with time.

GEOLOGIC SETTING

Stratigraphic and Structural History

The California borderlands west of the San Andreas fault have experienced a polygenetic tectonic evolution following cessation of subduction during early Miocene time including micro-plate capture, clockwise rotation of as much as 90°, and syn-tectonic volcanism (e.g., Kamerling and Luyendyk, 1979; Luyendyk et al., 1980; Nicholson et al., 1994; Weigand et al., 2002; Onderdonk, 2005), as well as oblique transpressional deformation related to the "Big Bend" of the San Andreas fault (e.g., Wright, 1991; Dolan et al., 1995; Shaw and Suppe 1996; Yeats, 1988). Thick sections of volcanic and volcaniclastic rocks of the Conejo and Topanga Formations accumulated in middle Miocene transrotational fault bounded basins, with Oligocene Sespe Formation on the up-thrown side (Fig. 3a) (e.g., Ehrenspeck, 1972; Willimas 1983; Ingersoll, 2001). Extensional deformation of the region continued until ca. 5 Ma, at which time development of the "Big Bend" of the San Andreas fault resulted in transpressional deformation and inversion of Miocene basins (e.g., Crowell, 1976; Wright, 1991). The modern structure and Quaternary shortening of the CFB is strongly influenced by the transrotational history as evidenced from reactivation of high-angle Miocene faults as west-striking high-angle reverse and north-striking transverse faults throughout the region (this study; Jakes, 1980; Yeats 1988).

Following Miocene extension and volcanism, deep-marine deposition in the Ventura basin (Fig. 1) ceased, and the basin was filled by a westward-thickening progradational sequence of Plio-Pleistocene turbidites, shallow marine sandstone and mudstone (Pico Fm.), and terrestrial sandstone and conglomerate (Saugus Fm.) (Fig. 3a). The age of the Plio-Pleistocene strata are calibrated by biostratigraphy, magnetostratigraphy, tephrochronology, and fission-track dating (*see* Yeats, 1988 *and the references therein*). Although the age of the Pico Formation and of the base of the Saugus Formation is known, the upper age limit of upper Pleistocene strata is unclear.

The Saugus Formation is a regionally extensive sedimentary unit (Fig. 1) that is interpreted to have been deposited by the ancestral Santa Clara River in response to tectonic uplift of the San Gabriel Mountains (e.g., Wright, 1991). Based on a single amino acid racimization (AAR) age near Ventura (Lajoie et al., 1982; Yerkes et al., 1987) and age estimates from sediment accumulation rates (Blackie and Yeats, 1976), the top of the Saugus Formation is thought to be between 400-200 ka, north of the CFB. The Saugus Formation is often the youngest unit involved in deformation in the Western Transverse Ranges and, therefore, better constraints on the source, lithology, thickness, timing, and distribution of this unit are needed to assess the magnitude and rate of deformation in this part of the Western Transverse Ranges.

Undeformed sedimentary units in the Ventura basin are typically considered younger than 200 ka and are given the name Quaternary older alluvium (Qoa or Qoal; e.g., Kew, 1924; Jakes, 1980; Dibblee and Ehrenspeck, 1992a, 1992b). These strata are often texturally and compositionally similar to Saugus strata.

Regional Tectonic Framework and Physiography

The CFB lies within the hangingwall of the north-thrusting Oak Ridge fault and south thrusting Malibu Coast fault (Fig. 1). Contractional deformation in southern California is the result of transpressive motion along a continental restraining bend in the San Andreas fault. Continuous GPS across the "Big Bend" of the San Andreas fault in southern California suggests high rates of shortening, with contractional deformation between Ventura and Los Angeles being 7-10 mm/yr (Donnellan et al., 1993; Argus et al., 1999). The structural grain of this part of the Western Transverse Ranges is characterized by east-west trending faults that accommodate left-oblique transpression and deform Cretaceous to upper Pleistocene aged strata into range-scale topography (e.g., Yeats, 1988; Walls et al., 1998; Meigs et al., 1999; Sorlien et al., 2006). Deformation in the CFB may be kinematically linked to deformation on the better-studied Oak Ridge fault (i.e., Gonzalez and Rockwell, 1991) or may represent a discrete seismic source area. Although no known earthquake surface ruptures exist within the CFB, prominent folds and fold scarps in upper Pleistocene to Holocene sediments, including those of the Oxnard Plain (delta of the Santa Clara River), attest to youthful deformation within the CFB.

The CFB is composed of several active and potentially-active east-west trending faults and folds that deform a topographic low between South Mountain to the north and the Santa Monica Mountains to the south (Fig. 2). Prominent folded strata are exposed in the Camarillo Hills north of the city of Camarillo and in the Las Posas Hills north of Santa Rosa Valley (Fig. 2). These hills are characterized by low relief (<250 m) south-verging anticlinal folds, which are developed above north-dipping reverse faults that are locally exposed at the surface but are commonly concealed beneath younger alluvium. Anticline forelimbs on the south flanks of folds typically dip more steeply (~35-90°) and are more incised than the more gently dipping backlimbs (~10-25°). The Camarillo and Las Posas Hills are separated by a water gap created by Calleguas Creek, which drains the Arroyo Las Posas and Arroyo Simi, both of which flow west out of Simi Valley (Fig. 2). An additional fault trend south of

the city of Camarillo and west of Calleguas Creek, herein referred to as the Camarillo anticline, uplifts fluvial strata into a low-relief (<25 m), undissected fold above the Oxnard Plain (CA, Fig. 2).

Previous Work in the Camarillo Fold Belt

Regional scale mapping by Kew (1924) documented the major folds and the Simi fault in the CFB and correlated all deformed post-Oligocene marine and non-marine bedrock to the Saugus Formation. Quaternary terrace deposits (Qt) were designated as undeformed but incised sediments. Utilizing subsurface petroleum data and new geologic mapping, Canter (1974) and Jakes (1980) conducted detailed subsurface analysis and generated cross sections across Big Mountain (Fig. 2) and the CFB, respectively, and included them in unpublished Masters theses. In both cases, post-Miocene shallow marine and terrestrial sandstone, siltstone, and conglomerate were given the name Saugus Formation. Their maps became the groundwork for published maps by Thomas Dibblee in the 1990s (e.g., Dibblee and Ehrenspeck 1990; 1992a, 1992b). Within the CFB, Dibblee and Ehrenspeck differentiated the marine and non-marine Saugus Formation of Jakes (1980) and Canter (1974), assigning the terrestrial sediments to the Saugus Formation and giving the name Las Posas Sand to marine sediments, which they correlated to the Pico Formation to the north (Fig. 4). These lithostratigraphic correlations have persisted and imply that Plio-Pleistocene terrestrial sedimentation in the CFB began ~2.5 Ma and continued until ~0.2- 0.4 Ma.

Within the CFB, Pleistocene strata thin from ~1200 m in the Oxnard plain near Camarillo (Jakes, 1990) to 900 m in the Happy Camp syncline, and they pinch-out discordantly against tilted Oligocene to Miocene strata on the south flank of the Big Mountain anticline (Figs. 2 and 4). To the south in the Las Posas Hills (Fig. 2), Pleistocene strata have a thickness <50 m and are characterized by a thin (<20 m) Las Posas Sand concordantly overlain by a terrestrial sequence of silty cobble conglomerate with interbedded soil horizons (Saugus of Dibblee and Ehrenspeck, 1990). The entire section of post-Miocene strata thickens westward (Jakes, 1980), yet the thickness of the upper terrestrial unit at the western tip of the Camarillo Hills does not exceed a thickness of 60 m (Q4; Fig. 4) (McNamara et al., 1991; Lopez, 1991; Kile et al. 1991). These studies in the Camarillo Hills did not note any evidence of surface beveling of the fold crest or erosional thinning of the terrestrial strata, which suggests the Pleistocene depositional history of this area was characterized by a protracted period of marine deposition followed by minimal accumulations of terrestrial strata.

The age of Pleistocene sedimentary rock in the CFB is poorly defined. A single AAR age in the Las Posas Hills collected from the marine Las Posas Sand indicates an approximate age of marine deposition of 450-700 ka in this part of the CFB (Boales, 1991) (Fig. 4). Although no absolute age dates exist for the younger terrestrial strata that overlie marine rocks in the CFB, a biostratigraphic age of 850-780 ka at the Moorpark mammoth site (Fig. 4) (Wagner et al., 2007) indicates that terrestrial sedimentation north of the CFB and Las Posas Valley may have begun significantly earlier than to the south, in the study area (Fig. 4).

Overlying the Saugus, the uppermost Pleistocene sedimentary units in the CFB are represented by a thin veneer of isolated and weakly dissected surficial deposits usually given the name Quaternary older alluvium (Qoa or Qoal; e.g., Jakes, 1980; Dibblee and Ehrenspeck, 1992). This older alluvium is composed of gravel and silt with "B" soil horizons (McCoy and Sarna-Wojcicki, 1979) and is nearly indistinguishable from so-named "Saugus" strata, from which it was previously differentiated by a perceived lack of deformation and/or weaker consolidation relative to Saugus beds (Jakes, 1980). These deposits are locally conformable and unconformable with the underlying strata (e.g., Dibblee and Ehrenspeck, 1992). No previous age data for these deposits exist.

METHODS OF INVESTIGATION

Geologic Mapping

Geologic mapping was concentrated on folded Oligocene to Pleistocene units exposed in the Las Posas and Camarillo Hills (Fig. 2). Previous geologic mappping from along the south flank of South Mountain and from localities where access was limited or where new urban development obscures bedrock exposures were utilized for this study (Kew, 1924, Jakes, 1980; Hanson, 1982, Dibblee and Ehrenspeck, 1990; Dibblee and Ehrenspeck, 1992, 1992a, 1992c; Yeats, 1988). North of the CFB, we field checked bedding attitudes along mapped fold axes in the Saugus Formation and focused on regions where young geomorphic surfaces and sedimentary units unconformably overlie Pleistocene to Oligocene bedrock. All mapping, data collection, and sample site locations were documented using a handheld computer running ESRI ArcPad with wireless GPS and plotted directly on orthographic photographs draped over high-resolution digital topography.

Previous stratigraphic nomenclature of Dibblee and Ehrenspeck (1992) were utilized for Oligocene to middle Pleistocene strata. Specifically, the name Las Posas Sand was used for Pleistocene marine deposits (QTlp) that unconformably overlie older Oligocene-Pliocene strata (Fig. 4). Terrestrial siltstones and conglomerates that everywhere overlie the Las Posas Sand, previously mapped as Saugus Formation (e.g., Jakes, 1980; Dibblee and Ehrenspeck, 1992, 1992a), are mapped as Q(1-5) based on absolute and inferred ages (Fig. 3b and Table 1).

Due to extensive agricultural use and urbanization of young geomorphic surfaces, sedimentary deposits Q3, Q2, and Q1 units (Fig. 3b) were correlated based on elevational continuity and topographic and geomorphic expression. Q3 is further divided into Q3a and Q3p. The designation Q3p is given to an extensive bedrock erosion surface with a thin veneer (< 4 m) of sediment that overlies the pediment in the eastern part of the study area. Locally, the Q3p deposits have been stripped; therefore, the underlying strath was mapped (Fig. 4). Q3a is given to coeval sediment to the west, where the underlying pediment surface either does not exist or is not exposed.

Geologic surface relations were then compared to more than 50 subsurface well data, compiled by Jakes (1980) and Canter (1974). Previous authors' lithologic interpretations of electronic logs and drill cores from well locations were relied upon

to 1) construct cross sections, 2) accurately locate subsurface structures, 3) determine fault and bedding dips, and 4) identify deformation on Miocene and Quaternary faults.

Geochronology

Optically stimulate luminescence (OSL) and radiocarbon geochronology was used to determine the age of deformed upper Pleistocene fluvial strata and to develop the Quaternary chronology and depositional history of this part of the Western Transverse Ranges. Samples were prepared and analyzed by Lewis Owen and Markus Fuchs at the University of Cincinnati. Determination of the age of the terrestrial strata, deformed in the CFB, is of critical importance to seismic hazard assessment in the Camarillo area, because the upper age of the formation is largely unknown. It is often the youngest unit deformed by faults and folds within the CFB. However, due to the high radiogenic dose rate of sediments in the CFB, OSL sample saturation occurs more rapidly than in other localities. Therefore, the maximum resolvable age by OSL in the CFB is ~ 45 ka (Appendix 2). Because the terrestrial strata in the CFB was thought to be Saugus equivalent and to be older than the age range of OSL dating, this geochronology investigation focused on younger deposits (Q1-Q3) and sedimentary accumulations in the western and southern margin of the field area (Q4) where previously mapped Saugus strata was likely the youngest.

This study includes 17 OSL analyses (Fig. 4 and Table 1) from samples that were collected from 3 paleoseismic trenches across the Camarillo anticline, deformed strata in the Springville anticline (Q4), sediment that overlie the Q3p erosion surface, and from Q2 sediment on the south flank of South Mountain (Fig. 4). The OSL technique records the elapsed time since sediment was last exposed to sunlight during transport and, therefore, the burial age. Up to 48 aliquots (on average 24) were measured for equivalent dose (D_e) estimation. All samples show a high D_e-scatter with a high percentage of measured aliquots already in saturation. The high D_e scatter can be explained by insufficient bleaching of the quartz grains during the last process of sediment reworking. A precise determination of the D_e from the quartz extracts was, therefore, not possible. Assuming insufficient bleaching of the quartz grains during their last sediment reworking, the lower part of the dose distribution might represent the best-bleached grains (*see review by* Murray and Olley, 2002). Therefore, a mean D_e was estimated from the lower part of the dose distribution. However, due to the close saturation of the samples, age estimates represent only a rough age approximation. Because water content affects dose rate, and water content since the time of burial can not be known and must be assumed, age estimates are present with 1σ error (Fuchs and Lang, 2001) (Table 1).

A single sample of woody debris was collected for radiocarbon analyses. Sample preparation and analysis was conducted at Beta Analytic Inc. Sample age is presented in before present (BP) calendar years with 2σ confidences (Table 1). One additional radiocarbon age collected from a paleoseismic trench in the CFB and limited soil chronologies taken from consulting reports are also presented.

RESULTS

Upper Pleistocene Stratigraphy

Geologic mapping and lithologic characterization for this study focused on the middle to upper Pleistocene terrestrial strata (Q1-4; Fig. 4) and their relations to the underling Las Posas Sand and Tertiary bedrock to characterize the late Pleistocene transpressive deformation within the CFB. A biostatigraphic age of ~780 ka at the Moorpark Mammoth site (Fig. 2; Wagner et al., 2007) suggests terrestrial strata on the south flank of South Mountain are coeval with and may, in fact, be Saugus Formation sourced from the San Gabriel Mountains. This correlation is supported by my geologic mapping north of the CFB, which locally identifies large cobble and boulder clasts composed of granitic and metamorphic rocks consistent with a source in the San Gabriel Mountains. However, in the CFB, clasts in Q4, previously mapped as Saugus Formation, are dominantly composed of pebbles consisting of Miocene Monterey Formation and Conejo volcanic clasts with less common granitic and metamorphic clasts. Monterey shale has a source both at South Mountain and to the south in the Santa Monica Mountains, where the volcanic clasts were derived. Pebbles are commonly found in a red-brown silty, massive matrix with no evidence of sorting or channelized flow. These deposits are intercalated with silty reddish paleosols that contain weak "B horizons" and carbonate cemented rhizoliths. The true thickness of these sediments is not known and may have been variable across the CFB. However, where the base and apparent top are exposed within fold of the CFB, terrestrial strata have a near uniform thickness of 40 - 60 m. Where exposed, Q4 strata are conformable with the underlying Las Posas Sand (McNamara et al., 1991, this study).

A thin veneer (<4 m) of fluvial sediments that unconformably overlie a planar erosion surface (Q3p) beveled on Sespe and Saugus Formations (Fig. 5) on the south flank of the Big Mountain anticline and along Calleguas Creek was mapped (Qoa of Dibblee, 1992a, 1992b). The Q3p surface dips ~1° to the southwest and extends from the south flank of Big Mountain, north of the city of Moorpark, westward to the approximate location of the town of Somis (Fig. 6). Typically, the deposit is massive and unbeded, being composed of coarse-grain sand and poorly-sorted cobble lag deposits that are compositionally identical to clasts found in the Sespe and Saugus Formations. Locally, these deposits contain large-scale trough cross-stratification (30 - 60 cm) and evidence of channelized flow. Coeval sediments exposed in paleoseismic trenches on the Camarillo anticline (Q3a, Fig. 4) are compositionally similar to those found overlying the erosion surface, but are commonly well-bedded (0.5 - 1 m) and composed of medium- to fine-grained sand and pebble conglomerate beds. The Q3a beds are differentiated from Q3p deposits based on absence of evidence that the underlying pediment surface is present beneath Q3a strata.

Latest Pleistocene deposits (Q2) are preserved east of the Wright Road fault and constitute the broad surface of the west Las Posas Valley (Figs. 2 and 4). Q2 sediments fill paleo-drainages along the south flank of South Mountain forming flat-floored valleys that locally extend to within 150 m of the range crest (Fig. 7). The Q2 unit is composed of massive greenish silt that contains fragments of Monterey shale.

These sediments are currently being incised by modern drainages and have a range of exposed thickness between 6 m and 15 m. The true thickness of this unit is not known and may vary along strike.

Geochronology

Q4 basal terrestrial strata

Our initial geochronology investigation of Q4 strata utilizing 4 quartz OSL analyses on samples collected from the Springville, Camarillo Hills, and Upland Road anticlines (Fig. 4). Two samples were collected from the western tip of the Springville anticline from two stratigraphic horizons to test reproducibility of the results. Due to saturation of the luminescence signal in quartz mineral separates from the Upland Road anticline and Camarillo Hills anticline only a minimum estimate of 45 ka could be assessed for Q4 strata at these sites using OSL methods (Samples 1-3, Table 1). The two samples collected from the Springville anticline gave inconsistent results with higher stratigraphic bed indicating saturation, while the lower bed gave an imprecise age of 35 ± 10 ka (samples 3 and 4, Table 1).

Due to saturation or near saturation of quartz samples, we utilized IRSL on feldspar mineral separates from the same sample sites that quartz separates were collected to determine the depositional age of the base of the Q4 deposits. IRSL age estimates from the base of Q4 strata indicate that terrestrial deposition began ca. 85 ka across the study area (Table 1).

The base of the terrestrial Q4 strata is exposed near the crest of the Upland Road anticline in a construction excavation (Fig. 4). At this site, several Q4 paleosols are exposed overlying a bivalve hash bed in the underlying Las Posas Sand. The paleosols dip gently south and are in the footwall of a south dipping thrust fault that uplifts and folds Las Posas Sand in the hangingwall. Q4 strata at this exposure have an IRSL age of 86 ± 6 ka (sample 7,Table 1).

The contact between the Las Posas Sand and Q4 strata in the Camarillo Hills is exposed in numerous drainages along the northlimb of the anticline. In contrast with northern backlimb, Q4 strata on the forelimb and crest of the Camarillo Hills anticline have been largely eroded away. Q4 strata on the backlimb dip 10°- 20° north, have a thickness of approximately 50 m, form planar dip slopes, and show no evidence of erosional beveling during uplift. An IRSL sample collected from the back limb of the Camarillo anticline from cross-bedded sand that that lay approximately 20 m upsection from the base of Q4 has an age of 78 ± 6 ka (sample 6, Table 1).

In the westernmost exposure of Q4 strata, in the nose of the Springville anticline, cross-bedded fluvial sand beds are tilled approximately 12° to the southwest and have an age of 84 ± 7 ka (sample 5, Table 1). Similar strata dip as much as 23° on the north limb of the anticline (Dibblee and Ehrenspeck, 1990; McNamara et al., 1991). Due to complete urbanization of the Springville anticline it is not possible to assess how far upsection these strata lie from the Las Posas Sand; but shell hash along the slopes near the sample site suggest the underlying marine strata are not deeply buried. During urban development, the Springville anticline was completely exposed, at

which time stratigraphic analysis by Lopez et al (1991) indicated that the thickness of terrestrial strata did not exceed 45 m and showed no evidence of erosion during tectonic uplift.

Late Pleistocene Erosion Surface (Q3p)

Three samples were collected for OSL analysis from the sediment overlying the Q3p erosion surface (Fig. 5). Samples 8 and 9 are separated by ~15 km (Fig. 4) and gave consistent ages of 26.9 ± 4.1 ka and 24.7 ± 2.0 ka, respectively (Table 1). Sample 10 is younger and gives an age of 19.2 ± 1.9 ka (Fig. 6). An additional age from sediments that overlie the Q3p surface comes from a paleoseismic trench, north of the Santa Rosa Valley fault (Fig. 4), which exposed south-dipping sediments that gave a radiocarbon age of 23.3 ± 1.0 ka (*see* Blake, 1991a *and the references therein;* Treiman, 1998). Geochronology of the Q3p sediments suggest a maximum depositional interval from 17-30 ka and a minimum interval from 21-23 ka.

Camarillo Anticline (Q3a strata)

Paleoseismic trenches across the crest and forelimb of the Camarillo anticline were excavated for the purpose of determining the magnitude of deformation along the Camarillo fault (Fig. 2). Trenches were logged by the managing consulting companies and field checked during OSL sample collection to determine the depositional environment and stratigraphic context of OSL age dates. The western Earth Systems trench site consisted of 2 excavations at the westernmost exposure of the anticline, from which we collected 3 OSL samples (Figs. 8a and 8b). Evidence of minor hangingwall deformation was observed in the trenches, but the Camarillo fault was not encountered. Two samples were collected within 3 m of each other from the southernmost tilted fluvial strata in trench A (Fig. 8). Strata strike N88W and dip 36°SE. OSL dates from samples 11 and 12 agree within error and give an age range from ~23-21 ka (Table 1). Sample 13 was collected from flat-lying silty-mud on the crest of the anticline and gave an older age of 32.3 ± 6.3 ka, suggesting the crest of the anticline experienced erosional beveling during early uplift, exposing lower stratigraphic units (Fig. 8b).

The eastern trench, located ~100 m east of the Earth Systems trench, was excavated by GeoSoils Inc. and consisted of a single trench, 100 m long and 15 m deep (Fig. 8c). Similar to the Earth Systems trench, the GeoSoils trench did not encounter the Camarillo fault. The trench extends from flat-lying strata at the crest of the Camarillo anticline, across the south-dipping forelimb and back into flat-lying strata south of the fold in the Oxnard plain (Fig. 10c). Four samples were collected and dated from the trench, all of which underlie a soil developed on the forelimb with an age estimate of ~30 ka (Shlemon, personal communication). Sample 14 came from a fluvial sand that strikes N80W and dips 36° south and gives an age of 27.8 ± 2.3 (Table 1). Samples of 16 and 17 came from the same bed and are within error and give an age range of ~27-32.5 ka (Table 1 and Fig. 8c). These samples are from an upper silty-mud unit, interpreted to be a colluvial wedge deposit that developed as a

result of tectonic uplift along the Camarillo anticline. Sample 18 comes from an upper colluvial deposit that overlies the former and gave an age of 40.8 ± 3.8 ka.

Samples 11-22 and 14-16 from the forelimb of the Camarillo anticline are all internally consistent and in good agreement with the soil chronology, indicating an age 20 - 30 ka for south-tilted strata in the forelimb of the Camarillo anticline. The older age given by sample 07, which is in disagreement with all other OSL dates and the soil chronology, is interpreted to be the result of insufficient bleaching and inheritance from lower stratigraphic units being exposed along the eroding anticlinal crest during uplift. Sample 15 gave an age of 18.3 ± 1.8 ka and comes from a flat-lying silty mud unit of the Oxnard plain that overlies fluvial sand at the southern extent of the trench (Fig. 8c). The strata from which sample 08 was collected appear to lie in the foreland of the Camarillo fault and are probably not involved in the deformation.

Latest Pleistocene alluvium (Q2)

Two OSL analyses were performed on samples collected from the Q2 unit. Both sample 19 and 20 come from back-filled valleys along the south flank of South Mountain (Fig. 7). Sample sites are separated by ~8 km and are both within 3 m of the geomorphic top of the Q2 unit at each locality (Fig. 7). The easternmost sample (sample 20) gave an age of 12.6 ± 1.4. Sample 19 gave an age of 4.8 ± 0.5 (Table 1).

Structural Domains

For this study, the CFB has been divided into four discrete structural domains. Domains are defined by fault segment boundaries and differences in the relative timing and style of deformation. Domains include: the Simi fault zone, the Santa Rosa fault zone, the Springville fault zone and the Camarillo fault zone (Fig. 9a). Fault segment boundaries are commonly occupied by north-striking faults that juxtapose lower stratigraphic units on the east against higher stratigraphic units on the west (Figs. 9a and 9b).

Simi Domain

The easternmost zone of faulting within the CFB contains the western extent of the well-studied Simi fault. East of the CFB (Fig. 1), the Simi fault delineates the northern extent of Simi Valley and the southern boundary of the Santa Susana Mountains and has been shown to have Quaternary slip (Hitchcock et al., 2001; Treiman, 1998). Within the CFB, the Simi fault zone is composed of several potentially active splays, including two northern segments and a southern concealed segment (Fig. 9a). The northern splays are exposed in the core of the east-trending Las Posas anticlinal ridge that is defined by a thin veneer (< 50 m) of east-striking oppositely dipping Las Posas Sand and Q4 strata (Fig. 1). Previous mapping of the northern Simi fault either shows the fault as a continuous structure or as a pair of right-stepping en echelon faults (Dibblee and Ehrenspeck 1990; Jakes, 1980, respectively) that dip steeply (75-85°) to the north. Although the fault is poorly exposed in parts of the Las Posas Hills, this study's geologic and geomorphic

mapping suggests that the fault is not continuous; insofar as such faults are depicted as a pair of right-stepping en echelon reverse faults (Fig. 9a).

All of the faults within the Simi domain show evidence of Miocene deformation. The northern Simi fault splays have opposite senses of Miocene dip-slip displacement. North of the northeastern Simi fault, the Saugus Fm. rests unconformably on north-dipping Oligocene Sespe Fm. (Ts), although, south of the fault, Q4 strata lie on Miocene rocks of the Topanga Fm. or Conejo volcanic rocks (Fig. 11a). In contrast, north of the northwestern Simi fault, Q4 rests on Miocene volcanic rocks and on Sespe Formation to the south (Figs. 9 and 10). The interpretation of Miocene dip-slip displacement on the Simi fault splays is consistent with previous mapping of the fault in north Simi Valley (Hanson, 1982, Dibblee and Ehrenspeck, 1992b). A cross section through the northern Simi fault splays, based on subsurface data and this study's mapping suggests a minimal amount of Quaternary reverse displacement on the northern fault segments (Fig. 10). These data suggest that the northern Simi faults may be involved in the folding and may locally accommodate a fraction of the contractional strain within the Las Posas anticline. However, the majority of Quaternary deformation of the Las Posas anticline is likely the result of folding and displacement on the southern splay of the Simi fault (Figs. 9a and 10; Santa Rosa fault of Treiman, 1998).

Similar to the northern strands, there is strong evidence of Miocene dip-slip displacement on the southern strand of the Simi fault. Subsurface wells on either side of the southern Simi fault show that the top of the Sespe Formation is displaced 1.6 km down in the south and overlain by a thick section of Topanga Fm. and Conejo volcanics (Figs. 10 and 11a). Based on projections of the base of the Las Posas Sand from well data, there may be as much as 100 m of Quaternary north-side-up displacement on the southern Simi fault (Fig. 10). The southern Simi fault intersects Shell Everett C-2 at ~600 m depth and must dip greater than 70° north, because it does not intersect Shell Everett #1 (Fig. 10). Although the southern splay of the Simi fault is concealed, a recent paleoseismic trench in the latest Pleistocene alluvial fan sediments, along the range front, shows evidence of faulting (Gurolla, personal communication, 2007).

The southern splay of the Simi fault offsets the north-striking East Barranca fault in the eastern Las Posas Hills (Fig. 9a). The East Barranca fault truncates the northern Simi fault and juxtaposes Q4 strata on the west against folded Sespe and Topanga Fms. within the Simi anticline to the east (Figs. 9). The Simi anticline plunges ~15° to the west and is truncated by the East Barranca fault. These relations suggest activity on the southern splay of the Simi fault west of the East Barranca fault postdates deposition of the base of Q4. Deformation within the Simi anticline east of the East Barranca fault likely resulted in uplift and removal of the Las Posas Sand and Q4 to the east. (Fig. 9). There is no evidence that the East Barranca fault deforms the Q3p surface in the northern Las Posas Hills. Either slip dies out to the north away from the Simi fault, or activation of the southern Simi within the CFB cut the East Barranca fault sometime before approximately 23 ka (age of Q3p). The southern splay of the

Simi fault in the CFB is likely the westward extension of the active Simi fault studied by Hitchcock et al. (1998) in the western Simi Valley.

All splays of the Simi fault and the west-plunging (15-20°) Las Posas anticline terminate to the west at a previously unmapped NNW-striking cross fault, herein referred to as the Camarosa fault (Fig. 9a). Similar to the Simi fault splays, the Camarosa fault appears to have an older Miocene and younger Quaternary deformational history. The fault is manifested by: 1) the truncation of most fault splays and folds to the east and west, 2) westward thickening of the Conejo/Topanga Fms., 3) subsurface juxtaposition of the Sespe Fm to the east against Topanga and Las Posas Sand to the west, 4) juxtaposition of the Q3p surface and the Q4 strata, 5) changes in the latest Pleistocene vertical uplift rates across the fault, and 6) distinct changes in the relative timing and geomorphic expression of faulting and folding (discussed later in GIS-based analysis).

East of the Camarosa fault, the top of the Sespe Fm is exposed at an elevation of 150 m and is overlain by a thin (~40 m) veneer of Topanga strata that is capped by Las Posas Sand and Q4. However, ~200 m to the west across the Camarosa fault, subsurface well data show the top of the Sespe Fm. is 350 m below sea level and overlain by ~500 m of Topanga strata (Fig. 11a). Post mid-Pleistocene transpressional deformation is characterized by ~90 m of uplift of the base of the Las Posas Sand (east-side-up) (Fig. 11b). This indicates that ~500 m of Miocene down to the west displacement occurred on the Camarosa fault before the east-side was uplifted ~90 m during the Quaternary, due to reverse faulting. In addition, separation of the Q3p surface and the long profile of Calleguas Creek increases by ~13 m to the west of the Camarosa fault, indicating post 23 ka differential uplift or down-cutting west of the Camarosa fault (Fig. 12).

Santa Rosa Domain

The Santa Rosa structural domain is bounded on its eastern margin by the Camarosa fault and on the west by the NNW-striking Somis fault. The domain is characterized by the largely undissected uplifted Q3p surface to the south, and by anticlinal folds in the Las Posas Sand and Q4 to the north (Fig. 9a). Four WSW-trending fault strands deform the domain. From north to south, they include: the northern Santa Rosa fault, the central Santa Rosa fault, the southern Santa Rosa fault, and the Santa Rosa Valley fault (Fig. 9a). Deformation along the northern, central, and southern Santa Rosa faults is topographically expressed within the west-plunging Upland Rd. anticline (Fig. 9a). Although the Upland Rd. anticline is densely urbanized and much of the traces of the Santa Rosa faults are concealed, the location and sense of displacement is known or can be inferred based on numerous paleoseismic trenches, subsurface well data and geomorphic expression. Previous paleoseismic trench logs show the northern and central Santa Rosa faults steeply dipping, with as much as 25 m of south-side up displacement of “younger alluvium” (probably Q4) (Tierra Tech, 1978; Buena Engineers, 1987; Boales, 1991). The northern and central splays are likely back-thrusts of the north-dipping southern splay

of the Santa Rosa fault and may accommodate a component of left-lateral deformation (Fig. 13).

The southern Santa Rosa fault juxtaposes Las Posas Sand and Q4 in the hangingwall against Q3p surface to the south (Figs. 9a and 13). Treiman (1998) interpreted an 18-27 m zone of brecciation and 5-8 times thickening of soil in a paleoseismic trench across the southern Santa Rosa fault as strong evidence for young displacement on the southern strand of the Santa Rosa fault. Topographic relief along the Upland Rd. anticline decreases from east to west along the southern Santa Rosa fault. The Upland Rd. antilcine has a well-defined west-plunging axis (Dibblee and Ehrenspeck, 1990; this study). However, the anticline does not plunge to the east and ends abruptly at the Camarosa fault (Dibblee and Ehrenspeck, 1990; Jakes, 1980; this study). Maximum topographic relief along the Upland Rd. anticline is approximately 65-70 m. Locally Q4 is completely removed from along the Upland Rd. anticline; however, exposures of Q4 along the forelimb and crest of the fold (Fig. 9a) suggest that significant erosion has not occurred (<40 m, see *Discussion*).

The specific structure that controls deformation along the West Las Posas anticline is less clear. No fault traces or surface offsets have been observed along this fold. However, the juxtaposition of Miocene volcanic rocks against Pre-Sespe strata in well logs from Texaco-Miketta#1 and southward thickening of Miocene strata (Fig. 13) suggest that a buried Miocene normal fault exists beneath the Santa Rosa domain. Similar to faults in the Simi domain, reactivation of this structure as a high-angle reverse fault may be controlling the Quaternary structural and morphologic development of the region. Similar to the Upland Rd. anticline, the West Las Posas anticline has a well-defined westward axial plunge, but ends abruptly at the Camarosa fault and does not plunge eastward (Dibblee and Ehrenspeck, 1990, this study). Maximum topographic relief of the West Las Posas anticline is approximately 140 m. Similar to the Upland Ridge anticline, the presence of Q4 along the crest and both fold limbs is interpreted to indicate that the topographic relief is a good proxy for structural relief (see *Discussion*).

South of the Santa Rosa faults, uplift and folding of the Q3p surface is the result of north-side-up displacement on the Santa Rosa Valley fault, which terminates to the east of the Camarosa fault (Figs. 9a and 13). Uplift of the Q3p surface along the Santa Rosa Valley fault has produced a 35 m scarp and open anticline (Santa Rosa Valley anticline) in the hangingwall of the fault. The uplifted Q3p surface in the hangingwall is nearly undissected to the west, becoming more dissected eastward. The eastern tip of the Santa Rosa Valley anticline, where it intersects the Camarosa fault is eroded away.

The Somis cross fault defines the western margin of the Santa Rosa domain. This fault is concealed beneath Holocene alluvium of Calleguas Creek. The Somis cross fault likely controls the position of the water gap between the Las Posas and Camarillo Hills. The fault was first mapped by Bailey (1951) and is shown as a down-to-the-west Miocene normal fault. Jakes (1980) used subsurface petroleum well data to argue for post-Miocene left-lateral offset on the Somis fault. Nowhere is the Somis fault exposed at the surface; determination of the pre-Quaternary sense of offset of

this fault is beyond the scope of this study. However, based on subsurface well data, significant post-middle Miocene tilting east of the Somis fault is apparent, whereas, west of the fault, Plio-Pleistocene strata are everywhere conformable with the underlying Miocene strata. This contrast may suggest that the Somis fault served as a tectonic boundary to late Miocene extensional deformation, separating discrete structural domains similar to the modern configuration. Evidence of Plio-Pleistocene activity on the Somis fault is best illustrated in a USGS Water Resources cross section based on water wells (Hanson et al., 2003). The cross section shows uplift and erosion of the upper Hueneme aquifer (Pico/Las Posas Fms.) east of the Somis fault beneath west Las Posas Valley, indicating Quaternary uplift east of the fault.

Springville Domain

West of the Somis fault and north of the city of Camarillo, the Camarillo Hills expose deformed Las Posas Sand and Q4 strata folded along the Springville fault zone (Fig. 9a). The Springville fault zone extends westward from Calleguas Creek for ~9 km, where it abruptly terminates in the Oxnard plain and the inferred Wright Rd. fault (Fig. 9a). Most of the faulting occurs along the south side of the hills and is concealed beneath younger alluvium. Deformation in the Camarillo Hills results in two discrete asymmetric south verging-anticlines within the Camarillo Hills: the Springville and Camarillo Hills anticlines (Fig. 9a). Dibblee and Ehrenspeck (1992a) depict the Springville fault zone as a continuous curvilinear north-dipping fault. However, Jakes (1980) proposed a southern Springville fault concealed below the Quaternary alluvium, based on subsurface offset of the upper Sespe Formation unconformity, observed in petroleum well cores. Both solutions are viable. However, this study depicts them as two discrete structures to enable a more clear and thorough discussion of the deformation associated with each fault. Therefore, geologic maps from this study show both a northern and southern strand of the Springville fault, although it is possible that these faults may be linked at depth and would be better characterized by single structure.

Bedding attitudes from the Camarillo Hills anticline clearly indicate the fold is doubly-plunging (this study; Jakes, 1980; Dibblee and Ehrenspeck, 1990), although the eastern extent has been modified by Calleguas Creek. In contrast, previous studies of the Springville anticline only document the west-plunging axis and do not show an east-plunging axis (Jakes, 1980; Dibblee and Ehrenspeck, 1990). The east-plunging nose may have been eroded away, unexposed at the time previous studies were conducted, or may have never formed. Unfortunately, due to extensive urbanization of the area, new investigations of the area are impractical, but based on several lines of evidence discussed later, it is probable that the east-plunging axis of the fold may never have existed.

The accommodation zone between the two east-trending anticlines is characterized by an ENE-trending topographic low. Drainage catchments developed within the accommodation zone are typified by west-flowing streams that drain the west-plunging axial trace of the Camarillo Hills anticline. In contrast, none of the watersheds developed on the Springville anticline drain eastward into the

accommodation zone, which may support the absence of an east-plunging fold axis. Whitney et al. (1991) documented abundant evidence within the accommodation zone of steep NE- and NW-trending tear faults with large lateral offsets in the area, and paleoseismic trenching within the accommodation zone identified a sub-vertical N15E trending fault whose inferred trace corresponds to the termination of both folds in the Camarillo Hills (Glenn, 1991). Therefore, it is possible that the accommodation zone between the northern and southern strands of the Springville fault may be characterized by a north-trending fault similar to other fault segment boundaries, in the CFB (e.g., the Camarosa fault).

As a result of urbanization of the Springville anticline, numerous consulting reports and geologic investigations have been completed on the southern Springville fault (*see* Blake et al., 1991a). However, the dip of the fault and magnitude of slip of the southern Springville fault are still debated. Jakes (1980) argues strongly for a steeply north-dipping fault (75-85°), based on subsurface data, in contrast with paleoseismic trench data that indicate surface fault dips of 15-45° (e.g., Kile et al., 1991; Ruff and Shlemon, 1991; Gonzalez and Rockwell, 1991). Based on previous work and this study's surface mapping of the fault trace, the southern Springville fault is interpreted to dip steeply (~70°) to the north, flattening to more gentle dips within a few 10s of meters of the surface, which may be common in inverted extensional basins (McClay and Buchanan, 1992) (Fig. 14).

Subsurface displacement estimates of the top of the Sespe Formation across the southern Springville fault suggest 275 m of north-side-up displacement (Jakes 1980), whereas the maximum displacement observed from paleoseismic trenching is only 10 m (Whitney and Gath, 1991). Given that the total topographic relief of the Springville anticline is only ~75 m, subsurface estimates suggest that a significant volume of Q4 strata should have been tectonically uplifted and eroded away. However, this possibility is inconsistent with the preservation of Q4 across the crest and forelimb of the fold, dip projections over the structure (Fig. 14), and a lack of observed erosion and unconformable deposits across the top of structure (McNamara, 1991). Offset of the top of the Sespe Formation is likely the result of Miocene down-to-the-south displacement, which is consistent with a 3-fold increase in the thickness of the Conejo volcanics and Topanga Fms. to the south (Fig. 14). Reactivation of this fault as a high-angle reverse fault has likely resulted in ~75 m of vertical uplift of the Springville anticline. At least some, if not all of this uplift occurred following the deposition of Q4 (<85 ka, Table 1).

Significantly fewer paleoseismic data exist for the northern Springville fault, and most of what can be derived comes from geologic mapping and subsurface well data. The fault zone along the south limb of the Camarillo Hills anticline is characterized by faceted spurs, steep to locally overturned Saugus strata on the southern forelimb, and deeply-incised drainages. Headward erosion of south-flowing drainages has driven the drainage divide north of the anticlinal axis and has exposed lower Las Posas Sand strata (Fig. 9a). The steeper dips and absence of terrestrial Q4 strata on the forelimb of the Camarillo hills anticline suggest a greater magnitude of folding and slip on this segment of the Springville fault zone. Based on topographic relief and

the thickness of exposed Q4 on the backlimb of the Camarillo anticline (35 m), which is similar to that described thickness along the Springville anticline (McNamara et al., 1991), it is estimated that the total vertical offset on the fault is between 150 m and 210 m.

The dip of the northern Springville fault is unknown. Based on a test pit across the northern strand, Bailey (1951) showed the fault dipping 25° to the north. However, the fault was not encountered in any of the deep petroleum wells to the north, indicating a steeper dip (75°; Jakes, 1980). Therefore, figure 14 illustrates two possible fault plane solutions.

The inferred Wright Rd. fault is characterized by a prominent 20 m-high topographic scarp that separates the Oxnard plain on the west and the latest Pleistocene Q2 surface Q2 of the west Las Posas Valley to the east (Fig. 9a). This location also corresponds to: 1) the abrupt westward termination of the Springville anticline, and 2) the location where shortening on the Oak Ridge fault goes to zero (Yeats and Huftile, 1995; Yeats 1988; Azor et al., 1988) as the Oak Ridge fault becomes more north-striking and is characterized by strike-slip displacement (Nicholson personal comm., 2008). The Wright Rd. fault has been hypothesized to exist by numerous consulting geologists and recommended for earthquake zoning by the California Geological Survey (Treiman, 1997). Pre-agricultural development photos show tonal lineaments suggestive of a low en echelon scarp in young sediments of the Oxnard plain that extends southward from the from the western tip of South Mountain toward the western tip of the Springville anticline. Although extensive cultivation of the region has modified the feature, a 2 m-high scarp can still be traced across the landscape most notably crossing Wright road near Beardsley Creek (this study, Treiman personal communication, 2007). This geologic and geomorphic evidence to suggests that the Wright Rd. fault may be responsible for the scarps in the Oxnard plain west of the west Las Posas Valley and likely limits the westward lateral growth of the Springville fault zone. Thus, the Wright Rd. fault may be related to deformation on the Oak Ridge fault.

Camarillo Domain

The Camarillo fault, which underlies the city of Camarillo, is manifested by the 3 km-long, 24 m-high east-trending anticline that plunges to the west beneath the Oxnard Plain. The fold terminates abruptly to the east and has likely been modified by Calleguas Creek (Fig. 2). The modern expression of the anticline is completely undissected in pre-development aerial photographs. However, truncation of the forelimb strata (strata 34-38, Fig 8c) indicates that a minimum of 10 m of erosional beveling of the crest of the Camarillo anticline occurred during the initial uplift of the fold near the westernmost topographic expression. Paleoseismic trenches indicate that the forelimb bedding planes dip as steep as 40°. Evidence of minor hangingwall deformation was observed in all trenches, but the Camarillo fault was not encountered. This indicates that slip on the Camarillo fault at the paleossiesmic sites is characterized by blind faulting. Total vertical uplift is estimated to be the sum of the modern relief (15 m) and the eroded thickness (10-15 m) from the crest,

indicating ~30 m of uplift related to fault propagation folding at the westernmost surface exposure of the Camarillo fault. If a similar amount of erosion occurred along the crest near the topographic high point, total vertical uplift may be as high as 40 m.

GIS-Based Analyses
(see previous Final Technical Report 07HQGR0040**)**

DISCUSSION

Sedimentation History

This research provides new insight into the erosional and depositional processes that shaped the landscape in this part of the Western Transverse Ranges. These processes are modulated by late Pleistocene to Holocene climate change and local tectonics. This investigation indicates that deposition of fluvial sands and conglomerates throughout the CFB, some of which were previously mapped as Saugus Formation, overlap in age with previously mapped younger alluvium (Qoa/Qoal Dibblee and Ehrenspeck, 1992& 1992a). Based on this study's geochronology, slip rate assessment, and limited sedimentologic study in the CFB, strata previously interpreted as Saugus (Q3a and Q4) in the study area are younger than 200 ka and are interpreted to be the result of local tectonics and source terrains, and not uplift of the San Gabriel Mountains.

Terrestrial Strata (Q4)

Locally, terrestrial strata that overlie the Las Posas Sand have been erosionally thinned; however, all active folds preserve the contact between marine and non-marine sediments on one or more of the fold limbs. Therefore, assessing the age of this datum, pre-tectonic original thickness, source, and genesis of Pleistocene terrestrial strata along strike of the CFB is critical to determining the magnitude and rate of fault-related uplift. The thickness of Pleistocene sediment is highly variable across the study area (Fig. 9b), yet the thicknesses of terrestrial strata are surprisingly uniform across the study area (30 - 60 m). Because the terrestrial strata are everywhere structurally concordant with the underlying Las Posas Sand, it is interpreted that Q4 strata are conformable with the underlying marine beds and were not deposited at any one locality during or after significant deformation occurred in the CFB. Consequently, terrestrial strata either represent 1) a thin progradational sequence of strata that everywhere cap marine deposits at the same stratigraphic level, 2) a remnant of a uniformly thicker sequence of terrestrial strata that has been uniformly thinned across the study area, or 3) a thicker section of strata, of non-uniform thickness that has been coincidentally thinned to 30 - 60 m across the study area. The available evidence suggests the first hypothesis is the most probable.

Field investigation of Q4 strata suggests these deposits were derived from South Mountain and the Santa Monica Mountains, and not from uplift of the San Gabriel Mountains (Saugus source terrain). Although clast counts were beyond the scope of this research, distinct differences exist between previously described Saugus strata and terrestrial strata within the CFB. Q4 strata are dominated by the presence of

Monterey shale and locally derived volcanic rocks and contain only minor plutonic clasts. This stands in contrast to Saugus strata described by numerous previous researchers and this study's investigation to the north, which show the Saugus Formation being dominated by the presence of granitic rocks, gneiss, metavolcanic, and quartzite, with only minor Monterey shale clasts (e.g., Dibblee and Ehrenspeck, 1992a). Uncommon granitic clasts identified within Q4 strata are interpreted to have been recycled from eroding Saugus strata on the south flank of South Mountain, which is believed to have been uplifted along the Oak Ridge fault sometime after 200-400 ka (Fig. 1) (Blackie and Yeats, 1976; Yeats, 1988). The volcanic clasts within the Q4 are Conejo volcanic clasts and were derived from the Santa Monica Mountains to the south, which have been exposed to sub aerial erosion since late Miocene time (Ingersoll, 2001).

Uplift of South Mountain would have resulted in isolation of the Camarillo area from the ancestral Santa Clara river that delivered sediment for the Saugus Formation deposited at South Mountain (Fig. 1). It seems likely that a narrow west-trending marine embayment would have developed between South Mountain and the Santa Monica Mountains at this time. Erosion of the Santa Monica Mountains and exposure of Saugus and Monterey shale on the flank of the rapidly uplifting South Mountain would have provided the appropriate sediment and clast lithology observed in Q4. Fine-grained silts and clays, paleosols, lack of evidence of channelized flow, and abundant root clasts overlying marine shell beds suggest that Q4 beds may represent deposition in a near shore floodplain, lagoonal, or estuarine environment. This interpretation is supported by Lopez (1991), who conducted a stratigraphic investigation of terrestrial strata exposed, in detail, during excavation for the Spanish Hills urban development on the Springville anticline.

Thus far, this study indicates that the onset of terrestrial deposition deformed in began at ~85 ka. To accurately assess the magnitude of vertical uplift on active structures, it is necessary to bracket the magnitude of surface denudation, and therefore, it is necessary to estimate the original thickness of Q4 strata. Unfortunately, this is not directly possible; but, based on field observations and several lines of reasoning, it appears terrestrial strata in the CFB have not been significantly thinned.

McNamara (1991) clearly stated that terrestrial strata had a thickness of ~60 m and that there was no evidence erosional beveling of deformed strata in the Springville anticline, which was completely exposed during urban development. Similarly, terrestrial strata along the back limb of the Camarillo Hills anticline are preserved as pristine unincised dip panels of similar thickness (~50 m) with no evidence of erosion. In addition, over the time interval of deposition of Q4 was deposited (~85-35 ka), sea level was at its lowest ~35 ky and was never more than 100 m below the elevation of the Camarillo area, which is located on the coastal piedmont. Therefore, even ignoring regional uplift of the Camarillo area in the hangingwall of the Oak Ridge and Malibu Coast faults over the past 200 ky, there is no reason to suspect that terrestrial strata would have ever exceeded 100 m in thickness. In fact, ~125 ky sea level (e.g., Lambeck and Chappell, 2001) was within 20 m of the modern elevation of the CFB. Based on these geologic and geographic

observations, it is clear that the 60 m of terrestrial strata observed in the westernmost part of the study is a reasonable thickness and likely reflects the maximum thickness of terrestrial strata in the study area.

Late Pleistocene Erosion Surface (Q3p)

Sediments overlying the Q3p erosion surface were dated using both OSL and radiocarbon analyses at four different localities, three of which gave consistent ages (22.7- 24.3 ka), while the fourth gave a slightly younger age (19.2 ± 1.9 ka) (Fig. 15). The age of these sediments must be younger than the underlying erosion surface, but by how much is unclear. Assuming that the age of the sediments place a close minimum limit on the age of bedrock planation (Mackin, 1937; Bull, 1990), then the age of the sediments should represent a time interval corresponding to the minimum length of time that the surface was active. In contrast, the overlying sediment may be significantly younger than the erosion surface, in which case the age of the sediment record aggradation and burial of the geomorphic surface. Regardless of the relationship between the geomorphic surface and the overlying sediments, the depositional age of the sediments is well constrained and, therefore, provides a valuable datum for assessing tectonic deformation since ~ 23 ka. However, it is probable that the sediments dated in this study reflect the age of surface cutting and, hence, the geomorphic surface itself is a valuable datum, even where the overlying sediments are not preserved.

The process, driving forces, and effects of geologic variability governing lateral bedrock planation and the genesis of pediments and strath terraces are still debated (e.g., Pazzaglia et al., 1998; Hancock and Anderson, 2002, Montgomery et al., 2004), indicating that the relationship of the erosion surface to the overlying sediment is also poorly understood. However, it is generally thought that sediments related to strath formation should be thin (one channel depth; Gilbert 1877; Mackin 1937). The Q3p sediment thickness is variable across the field area, and where exposed is ~2 m and always less than 4 m (Fig. 6). Although these thicknesses may seem excessive for a single channel depth, there is no clear evidence that these deposits accumulated by successive depositional events (e.g., intercalated soil profiles, bedding planes, scour and fill structures), which might suggest accumulation of Q3p sediments occurred over a protracted aggradational period. In contrast, the single massive bed, large-scale trough cross-stratification, and matrix supported coarse-grained cobble lags, which typify the Q3p deposit, are interpreted to reflect deposition during a single high-energy event. These sediments, therefore, likely represent the final pulse of sediment moving through the system, which were responsible for cutting the surface before the surface was abandoned at any particular locality. Consequently, the age of the sediment and the timing of activity on the erosion surface are likely closely linked.

Interpreting the age range of sediments that were being transported on the erosion surface presents another interesting challenge. Geochronology sample sites from Q3p sediment stretch across 24 km and suggest an interval of deposition from ~26 - 19 ka. This age range may reflect either the duration of bedrock planation or the timing of bedrock incision and abandonment of the transport surface. If the surface was more

constrained as within a narrow valley and was being acted upon by a single river system, it might be argued that the age of sediment overlying the strath better reflects the age of down-cutting and abandonment. However, the lack of confinement of the Q3p surface within defined valley walls and the broad area the surface (~45 km^2) argues against the entire surface being active at any one time. Therefore, the specific age of sediment deposited on the surface is interpreted to reflect the local timing of bedrock planation, and, thus, the range of ages indicates a minimum time that the surface was active.

Based on the available data, lateral bedrock planation and creation of the Q3p surface likely occurred during the interval from 26 - 19 ka. This interval falls within Marine Isotope Stage 2 (MIS2) and overlaps a period of low and relatively stable sea level, which was preceded by a 25 m precipitous drop in sea level that began ca. 30 ka. (Fig. 15) (Chappell et al., 1996; Lambeck and Chappell, 2001; Mix et al., 2001). Given the strong temporal correlation of these data to the last glacial maximum and environmental changes discussed below, it is probable that the genesis of the Q3p surface is climate-related rather than tectonic in origin. However, the exposure and preservation of the surface as isolated strath terraces is certainly the result of late Quaternary uplift.

The landscape's response to these changes in climate (e.g., aggradation vs. degradation) is complicated by numerous feedbacks between changes in precipitation, eustatic sea level, vegetation, runoff, rates of weathering, and a whole host of other environmental factors (see Bull, 1991). Several important climatic changes occurred in southern California at the transition between MIS3 to MIS2, including: 1) temperature suppression >5° C (Huesser, 1995), 2) contracted monsoonal conditions and the change from wet to drier conditions (Heusser 1995; Bird and Kirby, 2006; Kirby et al., 2006), and 3) a decrease in solar insolation and sea surface temperature (Berger and Loutre, 1991; Kennett et al., 1995) (Fig. 15). Perhaps the most significant change recorded in pollen records from the Santa Barbara channel is the steady change from pine/conifer forest to oak/juniper woodland from 26 ka to 19 ka (Fig. 20). Interpreted from this is a two-fold decrease in precipitation, from 100 cm/yr during MIS3 to <50 cm/yr during MIS2 (Fig. 15) (Huesser, 1995; 1998). It is important at this point to note that, although there was a 50% decrease in the rainfall between MIS3 and MIS2, precipitation during the last glacial maximum was 40% higher than modern mean annual precipitation (~30 cm/yr) in the study area. The decrease in precipitation and subsequent vegetation change over the interval 26 - 19 ka appears to have affected the fluvial system that, in part, led to the creation of the Q3p surface.

There is no evidence that the Q3p erosion surface extended west of the modern position of the water gap that Calleguas Creek flows through, south of the town of Somis (Fig. 2). However, coeval and compositionally similar sediment did accumulate south of the city of Camarillo (Q3a). Given the exposed thickness of these sediments in paleoseismic trenchs on the Camarillo anticline and the absence of the erosion surface, it appears that Q3a sediments represent a distal depositional facies of sediment being eroded from or transported on the Q3p surface. The downstream

change from lateral planation in the east to aggradation in the west likely reflects the paleotopogrpahy that existed at that time. Not dissimilar, perhaps, from today's topography, where uplifted bedrock to the east is eroded and transported by Calleguas Creek, and deposited in the Oxnard plain and Hueneme delta southwest if the city of Camarillo.

Uppermost Pleistocene Alluvium (Q2)

Two OSL age dates from the Q2 unit suggest an episode of aggradation in the study area that began sometime before 12.6 ka and extended until at least ~4.8 ka (Table 1). It is difficult to fully characterize the temporal and spatial patterns of deposition of these deposits, because only two data points exist that are separated by ~8 km in space and 8 ky in time (Fig. 4 and Table 1). If the onset of aggradation in the study area occurred at ~12 ka, this might suggest that the Q2 unit and infilling of incised canyons along South Mountain is the result of climate change related to the Pleistocene-Holocene transition (MIS2 to MIS1) (Fig. 15). Numerous studies have documented aggradation events in the Mojave Desert across this boundary (e.g., Melton, 1965; Ponti, 1985; Wells et al., 1987; Bull, 1991; Harvey et al., 1999). Less common are studies in southern California. However, Bull (1991) documented a sequence of fill terraces in south-flowing drainages in the San Gabriel Mountains (Fig. 1), which he interpreted to represent a period of aggradation that began approximately 14 ka and continued until 4 ka (Fig. 15).

Aggradation is thought to have resulted from a loss of vegetative cover and accelerated hillslope processes in response to the transition from a wetter late Pleistocene climate to a relatively dry semi-arid Holocene climate (e.g., Bull and Schick, 1979; Huesser, 1988; Bull, 1991). This time interval also corresponds to a period of eustatic sea level rise of ~50 m (Fig. 20) and vegetation change from juniper woodland to chaparral (Fig. 15). Strong correspondence of Q2 age dates with aggradation in the San Gabriel Mountains and in the Mojave Desert, rapidly rising sea level, and vegetation change all suggest that aggradation in this part of the western Transverse Ranges was the result of climate change at and following the Pleistocene-Holocene transition (Figs. 15).

In addition to distinguishing the timing of aggradation in the study area, the observed space-time relation between geochronology samples from the Q2 unit provide insight into the post-depositional timing of incision at their respective localities. There is no evidence of higher fill terraces in any of the drainages, nor evidence of degradation of the sediments near the top of the units that were sampled, so it is likely that the present geomorphic expression of the Q2 represents the maximum fill elevation. Yet, because both samples were collected within 3 m of the top of the Q2 unit but differed in age by ~8 ka, it is difficult to explain these ages based strictly on simple climatically driven aggradation and reincision models. Therefore, the age dates from the Q2 deposits likely reflect the effects of both tectonics and climate.

The paucity of data on the Q2 unit makes any tectonic interpretation tenuous. The eastern Q2 geochronology sample site, which yielded a depositional age of 12 ka, lies

very near the axis of the Long Canyon anticline, which deforms the south limb of the South Mountain anticline (sample 20, Fig. 4 and Table 1). It is reasonable to believe that local deformation along the structural axis of the fold may have promoted incision rather than deposition at the sample site. Approximately 15 m of incision at this locality is indicated by the separation between the top of Q2 and the modern stream. If the incision was driven completely by tectonic uplift this would suggest an uplift rate of ~1.3 mm/yr for the Long Canyon anticline. Alternatively, uplift and deformation along the axis of the fold may have resulted in erosional beveling of Q2 deposits and exposure of lower stratigraphic units, which may have been inadvertently sampled. Yet, because there was no evidence of deformation or erosion of the top of Q2 at this site, the former is preferred.

The eastern sample site yielded an age of ~4 ka (sample 19, Fig 4 and Table 1). At this locality, modern drainages are incised ~6 m. This suggests an incision rate of 1.5 mm/yr, similar to that at the eastern site. Although there is no known active structure near this site, it is possible that this rate reflects incision due to hangingwall uplift along the Oak Ridge fault. Alternatively, similar to aggradation in the San Gabriel Mountains, the end of aggradation and the return of degradation at 4 ka may reflect stabilization of hillslopes and climatically driven incision (Fig. 15) (Bull 1991).

Miocene Structural Inheritance

It is not known how many of the Quaternary faults in the study area are characterized by Miocene deformation; however, there is compelling evidence for Miocene slip on all strands of the Simi fault, Camarosa fault, and southern Springville faults. In almost all cases, the sense of Miocene slip on these faults is south side down with the interpreted controlling fault dipping steeply to the north (Figs. 10-12). These relations suggest either that Miocene deformation was characterized by a component of reverse dip-slip or that the faults have experienced horizontal-axis rotation, in addition to vertical-axis rotation (e.g., Kamerling and Luyendyk, 1979; Luyendyk et al., 1980). Although there is some local evidence of Miocene compression in the transverse ranges (Onderdonk personal comm.), the preponderance of research suggests that Miocene deformation was characterized by either transtension or transrotation (Kamerling and Luyendyk, 1979; Luyendyk et al., 1980; Nicholson et al., 1994; Ingersoll, 2001; Weigand et al., 2002). Therefore, it is concluded that reactivated Miocene faults, in the CFB, have experienced some amount of horizontal-axis rotation since the early Miocene.

Given the great magnitude of extensional deformation within the Western Transverse Ranges during the Miocene (e.g., Atwater, 1998; Weigand et al., 2001), it is not difficult to conclude that the faults in the CFB have undergone some degree of horizontal-axis rotation. In highly extended terrains, hangingwall rocks and faults commonly undergo horizontal-axis rotations during extension (e.g., Morton and Black, 1975; Proffett, 1977; Axen, 1988). The only requirement for Miocene faults in the CFB to have been rotated top-to-the-south would be for the region to have lain in the hangingwall of a coeval to younger north-dipping normal fault. This seems

probable, given that the study area is centrally located within the 75 km wide, transrotated domain of the western Transverse Ranges.

The magnitude of horizontal rotation of reactivated fault in the CFB is contingent upon the initial dip of these faults. If these faults formed in a transrotational tectonic regime that latter became transtensional, as Ingersoll (2001) suggests, the faults may have originally been steeply dipping, and, thus, a minimum of 15° of horizontal-axis rotation would be required to explain the current 75° northward dip of these faults. However, Nicholson et al. (1994) argued that early Miocene vertical-axis rotation was accommodated on transtensional faults, in which case >30° of horizontal-axis rotation would be required to explain the current fault orientations. Either possibility is plausible; however, based on hangingwall cutoff angles between interpreted Miocene faults and Conejo and Topanga strata, the former is preferred.

Where dip angles of Miocene strata are known from subsurface core data, cutoff angles are typically between 80° - 90°. The best example of this is in cross-section B'B' (Fig. 10), where the dip of the southern Simi fault is well known because it intersects well Shell Everett C-2 and is adjacent to 1.5 km thick section of Miocene strata that consistently dip 15° south. Back-rotation of the Miocene strata to the horizontal and equivalent rotation of the southern Simi fault would indicate that the fault was originally vertical, indicative of a transrotational origin. Similar relations can be seen in wells Texaco Miketta#1 and Burmah-Texaco Berlwood #3 (C-C', Fig. 12) and Texaco-Converse #1 (D-D', Fig. 13). Therefore, it is probable that several of the active Quaternary faults in the CFB are reactivated strike-slip faults that have experience as much as 15° of top to the south rotation about a horizontal axis.

GIS-based Analysis

(see previous Final Technical Report 07HQGR0040**)**

Earthquake Hazard and Fault Slip Rate Estimates

The principal objective of earthquake hazard assessment is to estimate the potential maximum magnitude of earthquake and recurrence interval for a particular fault. The seismic hazard posed by a fault is a function of: 1) the size of the fault, 2) its rate of slip, 3) the recurrence interval, 4) time since last earthquake, 5) the degree to which a fault fails in conjunction with neighboring faults, and 6) the range of earthquake sizes generated by a fault. This study places constraints on the first two parameters, the fault size and rate of slip. Moment magnitude estimates using regressions from global datasets from Wells and Coppersmith (1994) were calculated based on rupture length and modeled rupture area. However, because estimates of moment magnitude are empirically related to known geologic parameters and, therefore, affected by tectonic setting, we also utilized regression analysis of modeled fault plane area of Dolan et al. (1995). Their regression analysis was derived from data from southern California earthquake events and, thus, may better approximate potential earthquake magnitudes within the CFB, than do global datasets.

In order to estimate potential earthquake magnitudes for faults based on rupture area, it is necessary to assume a potential seismic source depth, determine fault length, estimate the fault dip and model the rupture area based on these parameters. Because several of the active faults, which intersect petroleum well at depth, dip ~75°, we utilize this angle for modeling fault plane area. Fault length is determined from the map trace of the fault. Rupture depth is based on historic earthquake rupture depths (>M_w 5.0) in the Western Transverse Ranges, which have typically occurred at depths between 8 – 17 km (Southern California Earthquake Catalog, http://www.data.scec.org/catalog_search/date_mag_loc.php). Therefore, we use a middle value of 12 km to model fault area (Table 2). Maximum variance of moment magnitude estimates based on modeled area for a 75° dipping fault plane between the preferred 12 km depth as compared to 17 km and 8 km is approximately M_w0.2. Faults that dip gently northward are assumed to intersect the south-dipping Oak Ridge fault above the seismogenic zone, and therefore are not considered discrete seismic source (e.g., Fig 13, northern Springville fault solution A). Similarly, the north-striking cross faults, which are oriented parallel to the regional stress direction, are not assumed to be seismic sources, but are likely to rupture coseismically during slip events on adjacent reverse faults (Fig. 16).

Ten fault segments are identified within the CFB that are Active (A), Apparently Active (AA), or Potentially Active (PA) (Table 2). Fault segment lengths are estimated, based on geometric, geomorphic, and structural discontinuities that indicate lateral fault termination at segment boundaries. Most fault segments are relatively short as a result of transverse faults, with the exception of the southern Simi fault which extends for ~ 18 km to the east of the CFB for a total length of 24 km (Table 2).

Potential moment magnitudes from the CFB are estimated to be within the range M_w 5.9 to M_w 6.7, with the southern Simi fault characterizing the largest hazard for the region (Table 2). A maximum moment magnitude of M_w 6.8 for the southern Simi might be expected if the fault was able to rupture through all the intervening transverse faults and link with the Santa Rosa and Springville fault zone.

Vertical fault slip rates are estimated, where good age determinations on deformed strata and geomorphic markers were available and assessment of the magnitude of pre-tectonic erosion across the uplifted topography was well constrained (Table 3). Yet, because the age of deformed strata are older than the deformation, fault slip estimates are only minimums. However, dated colluvial packages and underlying fluvial strata from paleoseismic trenches across the Camarillo anticline (Fig. 8) suggest that the age of tectonic tilting and the age of sedimentation are similar. Therefore, the interpreted fault slip rate estimates are likely robust.

The total topographic relief of folds is interpreted to represent the minimum vertical uplift due to fault related folding (Table 3). This study's preferred uplift estimates are derived from the summation of the known minimum vertical uplift estimated from topographic relief and the estimates of erosional thinning of terrestrial strata that overlie all active structures following uplift (see Sedimentation History).

The range of vertical fault slip rates are derived from the known or estimates of the age range of deformed terrestrial strata and the minimum and preferred magnitudes of offset (Table 3). The preferred rate is based on the preferred age estimate and preferred vertical uplift. Due to steep fault dips (75°), only vertical uplift rates are presented, which are inferred to closely approximate fault slip, at present (Table 3).

Fault Segment Boundaries and Transverse Faults

The Simi fault system extends for over 30 km from the northeastern side of Simi Valley to the Oxnard Plain. Of which, faults of the CFB characterize the highly segmented western extent of the deformation zone. It would be useful at this point to investigate more closely the deformation associated with the north-trending transverse faults which occupy most fault segment boundaries (Fig. 15) and which play an integral role in the lateral propagation of faulting and fault-related folding.

The north-striking orientation of the transverse faults, parallel to the regional shortening direction, would seem to suggest that transverse faults should have a large component of strike-slip movement and may represent tear faults. Although, accommodation of differential shortening by tear faulting may be common in compressional regimes (e.g., Twiss and Moores, 1992), in this study the non-genetic term transverse fault is used, because it was not possible to quantify the strike-slip component on these structures. In addition, the most compelling evidence of fault slip on transverse faults is the vertical component of deformation. However, it is probable that transverse fault are kinematically linked to the east trending reverse faults, have an oblique-reverse component of slip, and may locally transfer strain between adjacent structural domains.

Perhaps the most valuable insight into the deformation related to the transverse faults can be obtained from cross-section A-A' (Fig. 9b). The line of section is parallel to the deformational axis of the fold belt and orthogonal to known and inferred transverse faults (Fig. 9b). Constrained by subsurface data and illustrated in cross-section A-A' is a systematic decrease in structural relief from east to west across successive north-striking faults (East Barranca Rd., Camarosa, Somis, inferred, and Wright Rd. faults, respectively). The structural relief varies in both time and space, as shown by stratigraphic thickness changes in the Miocene Conejo and Topanga Fms. (Tcv-Tt), and the magnitude of offset of different age datum; specifically, the tops of the Pre-Sespe (Tps) and Sespe Formations (Ts), and the base of the Las Posas Sand (Qtlp). In all cases, the pattern is the same suggesting down to the south sense of displacement across the transverse faults.

Across the Camarosa and Somis faults, Miocene Conejo and Topanga strata thicken, and the top of the Sespe Formation increases in depth (Fig. 9b). These relations are interpreted to suggest that the Camarosa and Somis faults were both active during Miocene time and accommodated down to the west displacement. Hangingwall cut-off angles are sparse adjacent to the transverse faults but where present cutoff angles between 65-80°. This suggest, similar to the Simi and southern Springville fault, that transverse faults were originally strike-slip faults with a normal component or high angle normal faults that dipped steeply west. Post-Miocene offset

of the base of the Las Posas Sand is interpreted to be the result of Quaternary transpressional deformation (Fig. 9b). Therefore, similar to other Miocene faults in the study area, transverse faults have been reactivated and are accommodating some component of Quaternary shortening. Although the westward thickening of the Las Posas Sand complicates the determination of structural relief across the study area, structural relief across any one transverse fault should accurately reflect differential uplift at that locality.

If slip on the transverse faults is linked to deformation on adjacent reverse faults (Fig. 16), the local westward decrease in Quaternary structural relief across discrete transverse faults either reflects a westward decrease in the age or rate of faulting. As previously discussed, slip rate assessment suggests that the rates of deformation on active faults are similar across the fold belt (Table 3). Therefore, as concluded from the topographic analyses, the decrease in structural relief indicates westward propagation of deformation across transverse faults with the exception of the Somis fault.

Westward propagation of deformation is best constrained east of the Somis fault where there is good subsurface data and surface exposure to document the magnitudes and style of deformation on the Camarosa and East Barranca faults (Figs. 16 and 9b). Previous mapping of the Simi anticline north of Simi Valley (Fig. 2) show it extending for ~15 km east of the study (e.g., Dibblee and Ehrenspeck 1992b, Hanson, 1982) and ending 3 km east of the East Barranca fault. However, a prominent west-plunging anticline in Topanga and Sespe strata north of the southern Simi fault that terminates at the location of the East Barranca fault was mapped as a part of this study. Here, west-dipping Topanga and Sespe strata on the east are juxtaposed against north-dipping Las Posas Sand and Q4 strata to the west (Fig. 9a). Based on sediment thickness, ~70 m of east-side-up displacement (Fig. 9b) as a result of uplift and folding in the Simi anticline is indicated (Fig 9b). West of the fault, the Las Posas anticline is defined by north- and south-dipping Pleistocene strata. There is no evidence for eastward plunge of the Las Posas anticline. However, the axis of the fold plunges prominently westward east of the Camarosa fault where Oligocene to Miocene strata on the east are juxtaposed against Pleistocene strata on the west. Based on sediment thicknesses and well data, there is an estimated ~90 m of Pleistocene east-side-up differential uplift (Fig 9b and 11). Similar to the Las Posas anticline, there is no evidence of east-dipping strata or east plunging fold axes in the Upland Rd. or West Las Posas anticlines within the Santa Rosa domain.

Miocene to Quaternary Deformation

It is not known how many of the Quaternary faults in the study area are characterized by Miocene deformation; however, there is compelling evidence for Miocene slip on all strands of the Simi fault, Camarosa fault, and southern Springville faults (Fig. 9a). In almost all cases, the sense of Miocene slip on these faults is south side down with the interpreted controlling fault dipping steeply to the north. These relations suggest either that Miocene deformation was characterized by a component of reverse dip-slip or that the faults have experienced horizontal-axis rotation, in

addition to vertical-axis rotation. Although there is some local evidence of Miocene compression in the transverse ranges (Onderdonk *personal comm*., 2009), the preponderance of research suggests that Miocene deformation was characterized by either transtension or transrotation (Kamerling and Luyendyk, 1979; Luyendyk et al., 1980; Nicholson et al., 1994; Ingersoll, 2001; Weigand et al., 2002). Therefore, it is concluded that reactivated Miocene faults, in the CFB, have experienced some amount of horizontal-axis rotation since early Miocene time.

Given the great magnitude of extensional deformation within the Western Transverse Ranges during the Miocene (e.g., Weigand et al., 2001), it is not difficult to conclude that the faults in the CFB have undergone some degree of horizontal-axis rotation. In highly extended terrains, hangingwall rocks and faults commonly undergo horizontal-axis rotations during extension (e.g., Proffett, 1977; Axen, 1988). The only requirement for Miocene faults in the CFB to have been rotated top-to-the-south would be for the region to have lain in the hangingwall of a coeval to younger north-dipping normal fault. This seems probable, given that the study area is centrally located within the 75 km wide, transrotated domain of the western Transverse Ranges.

The magnitude of horizontal rotation of reactivated fault in the CFB is contingent upon the initial dip of these faults. If these faults formed in a transrotational tectonic regime that latter became transtensional, as Ingersoll (2001) suggests, the faults may have originally been steeply dipping, and, thus, a minimum of 15° of horizontal-axis rotation would be required to explain the current 75° northward dip of these faults. However, Nicholson et al. (1994) argued that early Miocene vertical-axis rotation was accommodated on transtensional faults, in which case >30° of horizontal-axis rotation might be required to explain the current fault orientations. Either possibility is plausible; however, based on hangingwall cutoff angles between interpreted Miocene faults and Conejo and Topanga strata, the former is preferred.

Where dip angles of Miocene strata are known from subsurface core data, cutoff angles are typically between 80° and 90°. The best example of this is in cross-section B-B' (Fig. 10), where the dip of the southern Simi fault is well known because it intersects well Shell Everett C-2 and is adjacent to 1.5 km thick section of Miocene strata that consistently dip 15° south. Back-rotation of the Miocene strata to the horizontal and equivalent rotation of the southern Simi fault would indicate that the fault was originally vertical, indicative of a transrotational origin. Similar relations can be seen in cross-sections other cross-sections across the CFB (DeVecchio, 2009). Therefore, it is probable that several of the active Quaternary faults in the CFB are reactivated strike-slip faults that have experience as much as 15° of top to the south rotation about a horizontal axis.

At present, these data cannot constrain the precise timing of deformation on discrete structures within the CFB. However, based on geologic mapping, geochronology investigation, and GIS-based analysis, it is possible to bracket the deformational timing on several of the active folds and faults and develop a relative chronology of deformation. For completeness, timing constraints of deformation

north of the CFB along South Mountain and Oak Ridge from previous studies are considered. The age of folded terrestrial strata places a maximum limit for inception of tectonic deformation at discrete localities and may closely reflect the actual timing. Figure 17 illustrates the approximate initiation time of deformation on previously discussed folds and faults in the CFB.

Although it is not known how many of the Quaternary faults in the study area are characterized by Miocene deformation, faults known to be reactivated are shown in Figure 17a. The oldest surficial evidence for pre-late Pleistocene folding in the study area is in the vicinity of the Oak Ridge and Big Mountain (Fig. 17b). There the Saugus Formation is deposited on a tilted section of pre-Pliocene bedrock on the south limb of the Big Mountain anticline, is conformable on the north limb with Pliocene Pico Formation, and thickens into the Happy Camp syncline to the north (Fig. 2). Conformity with the Pico Formation on the north limb of the anticline suggests that the unconformity on the south limb is the result of Miocene transtensional deformation and is not related to Plio-Pleistocene transpressive folding. Uplift of Big Mountain and down warping of the Happy Camp syncline must have begun after deposition of the base of the Saugus Formation. Although the precise age of the base of the Saugus Formation is not known at this locality, it is probably ~780 ka, based on the biostratigraphic age from Moorpark Mammoth site, which is near the base of the section. Folding in the Big Mountain area may have begun as early as ~780 ka and no later than deposition of the top of the Saugus (200-400 ka) (Fig. 17b).

Uplift of South Mountain began sometime after 200-400 ka (Fig. 17c) (Yeats, 1988; Blackie and Yeats, 1976). To the south, in the hangingwall of the north-dipping Simi fault, anticlinal folds within the Sespe and Topanga Formations are juxtaposed across the East Barranca fault against Pleistocene marine and terrestrial strata (Figs. 24c and 12b). Truncation of the Las Posas Sand to the west and its absence to the east suggests that the East Barranca fault was active either during or after the time of marine deposition in this part of the basin (<450-750 ka). The fault appears to have limited the westward growth of the western Simi anticline and accommodated up-to-the east displacement (Fig. 17c). The East Barranca fault was later cut by the southern strand of the Simi fault (Fig. 17d).

It is difficult of say when the onset of folding in the Camarillo Hills began. However, the similar degree of dissection, magnitude, and rate of vertical uplift suggest that deformation is coeval with the Las Posas anticline and slip on the Simi fault system (Figs. 18, 19 and Table 3).

Deformation in the Santa Rosa domain is complicated by the presence of several fault traces and folds of varying orientations. Based on previous analyses, deformation on the Upland Rd. and West Las Posas anticline began after deformation in the Simi domain (Fig. 17e), but sometime before uplift of t the Q3p surface on the Santa Rosa Valley fault. Lateral growth of the Simi fault into the Santa Rosa domain suggests that the Camarosa fault was truncated at this time, but the Camarosa fault appears to continue to affect eastward growth of the Santa Rosa Valley fault to the south.

Anticlinal folding and displacement on the Southern Springville fault is younger than 45 ka (Fig. 17e and Table 1). More youthful deformation on the southern strand of the Springville fault relative to the northern strand is further supported by topographic analyses and the youthful geomorphic expression of the Springville anticline. Latest Pleistocene fault slip rates on the southern Springville fault are estimated to be at least 1.6 mm/yr (Table 3). Both the Springville and South Mountain anticline terminate at the approximate location of the Wright Road fault. The Wright Road fault deforms Holocene sediments of the Oxnard plain and has up-to-the east sense of displacement and similar rates of uplift as the southern Springville fault (Table 3). The Wright Road fault is in the approximate location where the on-land segment of the Oak Ridge fault turns southward and becomes dominantly a strike-slip fault (Nicholson, personal comm., 2008). It is probable that the Wright Road fault may be related to this change in style of faulting and limits the westward lateral growth of the Springville fault into the Oxnard plain (Fig. 17e).

The youngest inferred folds in the fold belt are those that deform the youngest deposits (<30 ka) and those, which are characterized by weakly dissected uplifted surfaces (Fig. 24f). Paleoseismic trenches across the Camarillo fold clear indicate post-30 ka for that structure. Within the Santa Rosa domain, in the hangingwall of the Santa Rosa Valley fault, the Q3p surface is uplifted ~35 m above Calleguas Creek. Because changes in channel lithology cannot account for the 12 m increase in separation between Calleguas creek and the Q3p surface across the Camarosa fault (Fig. 14), it is interpreted to reflect increased down-cutting in response to post 23 ka higher uplift rates in the Santa Rosa domain. The absence of marine deposits underlying the Q3p suggests < 15 m of uplift occurred north of the Santa Rosa Valley fault before 23 ka.

CONCLUSIONS

This research represents an integrated application of geochronology, geology, and GIS-based analyses that bracket the timing of deformation on active folding within the CFB, places temporal constraints on the age of deformed terrestrial strata, and develops the Quaternary chronology of landscape evolution for this part of the Western Transverse Ranges. Optically stimulated luminescence and radiocarbon geochronology indicate that the age of terrestrial strata within the CFB are as young as ~25 ky. Strata in the CFB, previously mapped as Saugus Formation, are derived from the Santa Monica Mountains, and the Oak Ridge/South Mountain uplift and not the San Gabriel Mountains as previously suggested. Because uplift of the South Mountain area did not begin until 200-400 ka, all of the terrestrial strata in the CFB are younger than the upper age limit of Saugus strata to the north and east. These findings cast doubt on fault slip rate assessments of countless paleoseismic trench sites in the Western Transverse Ranges, which cite the presence of deformed Saugus strata.

The latest Pleistocene to Holocene landscape of this region of the Western Transverse Ranges was characterized by lateral planation of Oligocene to Pleistocene bedrock, followed by incision and aggradation. These processes are predominantly

the result of climate change and subsequent environmental effects on the fluvial system over the past 30 ky. Lateral planation of a regionally extensive erosion surface (Q3p) occurred between 26 - 19 ka, contemporaneous with Marine Isotope Stage 2 (MIS2). The Q3p surface would have covered an area covered >45 km^2 in the study area and may have extended to regions to the east and west. At present, it is preserved on the south flank of Big Mountain, near Moorpark, and as isolated strath terraces along Calleguas Creek. Abandonment of the Q3p surface occurred sometime after ~19 ka when streams began incising and cut deeply into the south flank of the Oak Ridge-South Mountain uplift. The incised drainages were later back-filled by as much as 20 m of hillslope-derived sediments (Q2) in response to climate change at the Pleistocene-Holocene boundary. These deposits are now being incised in the modern drainages.

Late Quaternary contractional deformation in the CFB is largely accommodated on reactivated Miocene transrotational strike-slip faults. North-striking transverse faults, some of which are inherited structures, have limited the lateral growth of faults and folds within the study area. Distinct changes in the magnitude, timing, rate, loci, orientation, and geometry of deformation across transverse faults indicate that cross faults impede deformation, which has implications for seismic hazard assessment. Systematic decreases in structural relief and the degree of topographic modification across any one transverse fault indicates that adjacent structural domains typically young to the west. Locally, transverse faults are cut by east-striking reverse faults. These observations demonstrate that transverse faults have a finite strength and result in punctuated lateral fault propagation. Holistically, folds within the CFB have grown within the last 200 ky and young to the south and west. Where that age of deformed strata and geomorphic markers is well known, vertical uplift rates of ~1.5 mm/yr are typical, which is three times greater than previous rates from paleoseismic studies. For the southern Simi fault, which is the oldest, longest, most continuous structure, with the greatest magnitude of deformation, a maximum moment magnitude of M_w6.8 might be expected if the entire fault zone were to rupture.

REFERENCES

Anderson, D. E., Wells, S.G.,, 2003, Latest Pleistocene lake highstands in Death Valley, California: Special Paper - Geological Society of America, v. 368, p. 115-128.

Argus, D. F., Heflin, M. B., Donnellan, A., Webb, F. H., Dong, D., Hurst, K. J., Jefferson, D. C., Lyzenga, G. A., Watkins, M. M., and Zumberge, J. F., 1999, Shortening and thickening of metropolitan Los Angeles measured and inferred by using geodesy: Geology (Boulder), v. 27, no. 8, p. 703-706.

Axen, G. J., 1988, The geometry of planar domino-style normal faults above a dipping basal detachment: Journal of Structural Geology, v. 10, no. 4, p. 405-411.

Azor, A., Keller, E.A., and Yeats, R.S., 2002, Geomorphic indicators of active fold growth; South Mountain-Oak Ridge Anticline, Ventura Basin, Southern California: Geological Society of America Bulletin, v. 114, p. 745-753.

Bailey, T.L., 1951, Geology of a portion of Ventura Basin: unpublished map

Berger, A., and Loutre, M. F., 1991, Insolation values for the climate of the last 10 million years: Quaternary Science Reviews, v. 10, no. 4, p. 297-317.

Bird, B. W., and Kirby, M. E., 2006, An alpine lacustrine record of early Holocene North American monsoon dynamics from Dry Lake, Southern California (USA): Journal of Paleolimnology, v. 35, no. 1, p. 179-192.

Blackie, G. W., and Yeats, R. S., 1976, Magnetic-reversal stratigraphy of Pliocene-Pleistocene producing section of Saticoy oil field, Ventura Basin, California: AAPG Bulletin, v. 60, no. 11, Part 1, p. 1985-1992.

Blake, T. F., 1991a, Synopsis of the character and recency of faulting along the Simi-Santa Rosa fault system: in Engineering Geology along the Simi-Santa Rosa fault system and adjacent areas, Simi Valley to Camarillo Ventura County, California, *in* Blake, T. F., ed., Annual field trip guidebook Southern California Section Association of Engineering Geologists, v. 1., p. 96-118.

Blake, T. F., 1991b Engineering Geology along the Simi-Santa Rosa fault system and adjacent areas, Simi Valley to Camarillo Ventura County, California. Annual field trip guidebook Southern California Section Association of Engineering Geologists, 2v., 383 p.

Boales, P. V., 1991, Near-surface geology of the southwestern Las Posas Hills area, Camarillo, Ventura County, California, *in* Blake, T. F., ed., Engineering Geology along the Simi-Santa Rosa fault system and adjacent areas, Simi Valley to Camarillo Ventura, California, p. 230-243.

Brozovic, N. B., D W; Fielding, E J F; Meigs, A J, 1995, The spatial and temporal topographic evolution of Wheeler Ridge, California; new insights from digital elevation data: Geological Society of America Abstracts with Programs, v. 27, no. 6, p. 396.

Buena Engineers, 1987, Geologic report for Tract 4296, Camarillo, California, (unpublished consultant report).

Bull, W. B., and Schick, A. P., 1978, Impact of climatic change on an arid watershed: Abstracts with Programs - Geological Society of America, v. 10, no. 3, p. 98.

Bull, W. B., 1990, Stream-terrace genesis; implications for soil development: Geomorphology, v. 3, no. 3-4, p. 351-367.
Bull, W. B., 1991, Geomorphic responses to climatic change.
Bucher, W. H., 1932, "Strath" as a geomorphic term: Science, v. 75, p. 130-131.
Canter, N. W., 1974, Paleogeology and paleogeography of the Big Mountain area, Santa Susana, Moorpark, and Simi Quadrangles, Ventura County, California: Ohio University at Athens, Athens, OH, United States (USA).
Carroll, A. R., and Bohacs, K. M., 1999, Stratigraphic classification of ancient lakes; balancing tectonic and climatic controls: Geology, v. 27, no. 2, p. 99-102.
Chappell, J., Omur, A., Esat, T., McCulloch, M., Pandolfi, J., Ota, Y., Pillans, B., 1996, Reconciliation of late Quaternary sea levels derived from coral terraces at Huon Peninsula with deep sea oxygen isotope records, Earth and Planetary Science Letters, vol. 141, p. 227-236.
Chen, Y., Sung, Q., Cheng, K. (2003) Along-strike variations of morphotectonic features in the western foothills of Taiwan; tectonic implications based on stream-gradient and hypsometric analysis. Geomorphology, vol. 56 no.1-2, p. 109-137. doi:10.1016/S0169-555X(03)00059-X.
Crowell, J. C., 1976, Implications of crustal stretching and shortening of coastal Ventura Basin, California: Miscellaneous Publication (American Association of Petroleum Geologists Pacific Section), no. 24, Aspects of the geol. hist. of the Calif. Cont. Borderland, p. 365-382.
Davis, T. L., Namson, J., Yerkes, R. F., 1989, A cross section of the Los Angeles area: Seismically active fold and thrust belt, the 1987 Whittier Narrows earthquake, and earthquake hazard, Journal of Geophysical Research, vol. 94, p. 9644-9664.
Dibblee, T. W., Ehrenspeck, H. E., Thomas W. Dibblee Jr. Geological Foundation., California. Division of Mines and Geology., and Geological Survey (U.S.), 1990, Geologic map of the Camarillo and Newbury Park quadrangles, Ventura County, California: Dibblee Geological Foundation, scale 1:24,000.
Dibblee, T. W., Ehrenspeck, H. E., California. Division of Mines and Geology., Geological Survey (U.S.), and Thomas W. Dibblee Jr. Geological Foundation., 1992a, Geologic map of the Moorpark quadrangle, Ventura County, California: Dibblee Geological Foundation, scale 1:24,000.
Dibblee, T. W., Ehrenspeck, H. E., Thomas W. Dibblee Jr. Geological Foundation., California. Division of Mines and Geology., and Geological Survey (U.S.), 1992b, Geologic map of the Simi quadrangle : Ventura County, California: Dibblee Geological Foundation ; Division of Mines and Geology distributor, scale 1:24,000.
Donnellan, A., Hager, B. H., and King, R. W., 1993, Discrepancy between geological and geodetic deformation rates in the Ventura Basin: Nature, v. 366, no. 6453, p. 333-336.
Dolan, J. F., Sieh, K., Rockwell, T. K., Yeats, R. S., Shaw, J., Suppe, J., Huftile, G. J., and Gath, E. M., 1995, Prospects for larger or more frequent earthquakes in the Los Angeles metropolitan region: Science, v. 267, no. 5195, p. 199-205.

Dolan, J. F., Sieh, K., Rockwell, T. K., Guptill, P., and Miller, G., 1997, Active tectonics, paleoseismology, and seismic hazards of the Hollywood fault, northern Los Angeles basin, California: Geological Society of America Bulletin, v. 109, no. 12, p. 1595-1616.

Dolan, J. F., and Rockwell, T., 2001, Paleoseismic evidence for a very large (M (sub w) >7), post-A.D. 1660 surface rupture on the eastern San Cayetano Fault, Ventura County, California; was this the elusive source of the damaging 21 December 1812 earthquake?: Bulletin of the Seismological Society of America, v. 91, no. 6, p. 1417-1432.

Dolan, J. F., Christofferson, S. A., and Shaw, J. H., 2003, Recognition of paleoearthquakes on the Puente Hills blind thrust fault, California: Science, v. 300, no. 5616, p. 115-118.

Dyke, A. S., Moore, A., and Robertson, L., 2003, Deglaciation of North America: Geological Survey of Canada, 1574.

Ehrenspeck, H. E., 1972, Geology and Miocene volcanism of the eastern Conejo Hills area, Ventura County, California [Thesis M A --University of California Santa Barbara 1972 thesis], vii, 135 leaves, bound. p.

El Hamdouni, R., Irigaray, C., Fernandez, T., Chacon, J., & Keller, E. A. 2008, Assessment of relative active tectonics, southwest border of the Sierra Nevada (southern Spain). Geomorphology, vol. 96, no. 1-2, p. 150-173. doi:10.1016/j.geomorph.2007.08.004.

Fletcher, J., Spelz-Madero, R., & Owen, L. (2007). Origin of megamullion corrugations and evolution of a rolling hinge: Insights from a morphometric and structural analysis of an active low-angle normal fault, sierra el mayor, baja california; geological society of america, 2007 annual meeting. Abstracts with Programs - Geological Society of America, vol. 39, no.6, p.184.

Formento-Trigilio, M. L., Burbank, D. W., Nicol, A., Shulmeister, J., and Rieser, U., 2003, River response to an active fold-and-thrust belt in a convergent margin setting, North Island, New Zealand: Geomorphology, v. 49, no. 1-2, p. 125-152

Gilbert, G. K., 1877, Report on the lithologic character of the Henry Mountains, Government Printing office, 160 p.

Glenn, D., 1991, A fault trenching study along the Springville fault zone, Camarillo, California, *in* Blake, T. F., ed., Engineering Geology along the Simi-Santa Rosa fault system and adjacent areas, Simi Valley to Camarillo, Ventura, California, p. 205.

Gurrola, L. D., Keller, E. A., and Anonymous, 1999, Seismic hazards of the Santa Barbara fold belt, California: Abstracts with Programs - Geological Society of America, v. 31, no. 7, p. 474.

Gonzalez, T., and Rockwell, T. K., 1991, Holocene activity of the Springville Fault in Camarillo, Transverse Ranges, Southern California; preliminary observations: *in* Blake T. F., ed., Engineering Geology along the Simi-Santa Rosa fault system and adjacent areas, Simi Valley to Camarillo Ventura County, California. Annual field trip guidebook Southern California Section Association of Engineering Geologists, v. 2, p. 396-383.

Gurrola, L. D., Keller, E. A., and Anonymous, 1999, Seismic hazards of the Santa Barbara fold belt, California: Abstracts with Programs - Geological Society of America, v. 31, no. 7, p. 474.
Hancock, G. S., and Anderson, R. S., 2002, Numerical modeling of fluvial strath-terrace formation in response to oscillating climate: Geological Society of America Bulletin, v. 114, no. 9, p. 1131-1142.
Hanson, D. W., 1982, Surface and subsurface geology of the Simi Valley area, Ventura County, California: Oregon State University, Corvallis, OR, United States (USA).
Hanson, R.T., Martin, P., Koczot, K.M., 2003, Simulation of Ground-Water/Surface-Water Flow in the Santa Clara–Calleguas Ground-Water Basin, Ventura County, California, U.S. Geological Survey Water Resources Report, 157 p.
Hauksson, E., Jones, L. M., and Hutton, K., 1995, The 1994 Northridge Earthquake Sequence in California - Seismological and Tectonic Aspects: Journal of Geophysical Research-Solid Earth, v. 100, no. B7, p. 12335-12355.
Harvey, A. M., Wigand, P. E., and Wells, S. G., 1999, Response of alluvial fan systems to the late Pleistocene to Holocene climatic transition; contrasts between the margins of pluvial lakes Lahontan and Mojave, Nevada and California, USA: Catena (Giessen), v. 36, no. 4, p. 255-281.
Heusser, L., 1995, Pollen stratigraphy and paleoecologic interpretation of the 160-K.Y. Record from Santa Barbara Basin, Hole 893A. Santa Barbara Basin, California: Proceedings of the Ocean Drilling Program, Scientific Results, v. 146, no. 2, p. 265-279.
Heusser, L., 1998, Direct correlation of millennial-scale changes in western North American vegetation and climate with changes in the California current system over the past approximately 60 kyr: Paleoceanography, v. 13, no. 3, p. 252-262.
Hitchcock, C. S., Treiman, J. A., Lettis, W. R., Simpson, G. D., and Anonymous, 1998, Paleoseismic investigation of the Simi Fault at Arroyo Simi, Simi Valley, Ventura County, California: Abstracts with Programs - Geological Society of America, v. 30, no. 5, p. 19-20.
Hughes, T. J., Denton, G. H., Andersen, B. G., Schilling, D. H., Fastook, J. L., and Lingle, C. S., 1981, The last great ice sheets; a global view.
Ingersoll, R. V., 2001, Tectonostratigraphy of the Santa Monica Mountains, Southern California. Guidebook - Pacific Section, American Association of Petroleum Geologists, p. 63-70.
Jakes, M. C., 1980, Surface and subsurface geology of the Camarillo and Las Posas Hills area, Ventura County, California: Oregon State University, Corvallis, OR, United States (USA).
Kamerling, M. J., and Luyendyk, B. P., 1979, Tectonic rotations of the Santa Monica Mountains region, Western Transverse Ranges, California, suggested by paleomagnetic vectors: Geological Society of America Bulletin, v. 90, no. 4, p. I 331-I 337.
Kennett, J. P., Baldauf, J. G., Behl, R. J., Bryant, W. R., Fuller, M., Grimm, K., Heusser, L., Kemp, A. E. S., Lange, C. B., Lund, S. P., Merrill, R. B., Olivier, F.,

Polgreen, E., Pratt, L. M., Rack, F. R., Schimmelmann, A., Schwartz, M., Stein, R., Thurow, J., and Musgrave, R. J., 1995, Latest Quaternary benthic oxygen and carbon isotope stratigraphy; Hole 893A, Santa Barbara Basin, California: Proceedings of the Ocean Drilling Program, Scientific Results, v. 146, no. 2, p. 3-18.

Keller, E. A., Pinter, N., 2003, Active Tectonics; earthquakes, uplift, and landscape, 1st ed., 362 pp., Prentice Hall, Upper Saddle River, NJ.

Kew, W. S. W., 1924, Geology and oil resources of a part of Los Angeles and Ventura counties, California, B 0753.

Kile, M. B., McMillan, K., McNamara, J.E, Primas, T.M., Butler, G, 1991, Structural Geology of the westernmost Camarillo Hills, Ventura County, California, *in* Blake, T. F., ed., Engineering Geology along the Simi-Santa Rosa fault system and adjacent areas, Simi Valley to Camarillo, Ventura, California.

Kirby, M.E., Lund, S.P., and Bird, B.W., 2006, Mid-Wisconsin sediment record from Baldwin Lake reveals hemispheric climate dynamics (Southern CA, USA): Palaeogeography, Palaeoclimatology, Palaeoecology, v. 241, p. 267-283.

Kirby, M. E., Lund, S. P., Anderson, M. A., and Bird, B. W., 2007, Insolation forcing of Holocene climate change in Southern California; a sediment study from Lake Elsinore: Journal of Paleolimnology, v. 38, no. 3, p. 395-417.

Lajoie, K. R., Sarna-Wojcicki, A. M., Yerkes, R. F., and Cooper, J. D., 1982, Quaternary chronology and rates of crustal deformation in the Ventura area, California.

Lambeck, K., Chappell, J., Smith, J., and Uppenbrink, J., 2001, Sea level change through the last glacial cycle: Science, v. 292, no. 5517, p. 679-686.

Larsen, S. C., Agnew, D. C., and Hager, B. H., 1993, Strain Accumulation in the Santa-Barbara Channel - 1970-1988: Journal of Geophysical Research-Solid Earth, v. 98, no. B2, p. 2119-2133.

Lopez, W. B., 1991, Depositional environments and provenance of the Saugus and San Pedro Formations, Las Posas and Camarillo Hills area, Ventura County, California, *in* Blake, T. F., ed., Engineering Geology along the Simi-Santa Rosa fault system and adjacent areas, Simi Valley to Camarillo, Ventura, California.

Luyendyk, B. P., Kamerling, M. J., and Terres, R., 1980, Geometric model for Neogene crustal rotations in southern California: Geological Society of America Bulletin, v. 91, no. 4, p. I 211-I 217.

Mackin, J. H., 1937, Erosional history of the Big Horn Basin, Wyoming [Doctoral thesis]: Columbia University.

Mackin, J. H., 1948, Concept of the graded river: Geological Society of America Bulletin, v. 5, p. 463-511.

McClay, K. R., and Buchanan, P. G., 1992, Thrust faults in inverted extensional basins, Chapman & amp; Hall, London, United Kingdom (GBR).

McCoy, G., and Sarna-Wojcicki, A. M., 1978, Preliminary map showing surficial materials of the Ventura-Oxnard Plain area, California: U. S. Geological Survey, OF 78-1065.

McNamara, J. E., McMillan, K., Lopez, W.B., Kile, M.B., Butler, G., Van Alstine, D., 1991, Saugus Formation stratigraphy, Camarillo Hills, Ventura County, California, *in* Blake, T. F., ed., Engineering Geology along the Simi-Santa Rosas fault system and adjacent areas, Simi Valley to Camarillo, Ventura, California.

Melton, M. A., 1965, The geomorphic and paleoclimatic significance of alluvial deposits in southern Arizona: Journal of Geology, v. 73, no. 1, p. 1-38.

Meigs, A., Brozovic, N., and Johnson, M. L., 1999, Steady, balanced rates of uplift and erosion of the Santa Monica Mountains, California: Basin Research, v. 11, no. 1, p. 59-73.

Mix, A. C., Bard, E., and Schneider, R., 2001, Environmental processes of the ice age; land, oceans, glaciers (EPILOG): Quaternary Science Reviews, v. 20, no. 4, p. 627-657.

Mitchum, R. M., Jr., Vail, P. R., and Sangree, J. B., 1977, Seismic stratigraphy and global changes of sea level; Part 6, Stratigraphic interpretation of seismic reflection patterns in depositional sequences.

Montgomery, D. R., 2004, Observations on the role of lithology in strath terrace formation and bedrock channel width: American Journal of Science, v. 304, no. 5, p. 454-476.

Murray, A. S. and Olley, J. M., 2002, Precision and accuracy in the optically stimulated luminescence dating of sedimentary quartz: A Status review, Journal on Methods and Applications of Absolute Chronology, Geochronometria, vol. 21, p. 1-16.

Nicholson, C., Sorlien, C. C., Atwater, T., Crowell, J. C., and Luyendyk, B. P., 1994, Microplate capture, rotation of the Western Transverse Ranges, and initiation of the San Andreas transform as a low-angle fault system: Geology (Boulder), v. 22, no. 6, p. 491-495.

Nicol, A., Walsh, J., Berryman, K., and Nodder, S. D., 2005, Growth of a normal fault by the accumulation of slip over millions of years: Journal of Structural Geology, v. 27, no. 2, p. 327-342

Onderdonk, N. W., Minor, S. A., and Kellogg, K. S., 2005, Taking apart the Big Pine Fault; redefining a major structural feature in Southern California: Tectonics, v. 24, no. 6, p. 11.

Oskin, M., Sieh, K., Rockwell, T., Miller, G., Guptill, P., Curtis, M., McArdle, S., and Elliot, P., 2000, Active parasitic folds on the Elysian Park anticline: Implications for seismic hazard in central Los Angeles, California: Geological Society of America Bulletin, v. 112, no. 5, p. 693-707.

Ponti, D. J., 1985, The Quaternary alluvial sequence of the Antelope Valley, California: Special Paper - Geological Society of America, v. 203, p. 79-96.

Kirby, M. E., Lund, S. P., and Bird, B. W., 2006, Mid-Wisconsin sediment record from Baldwin Lake reveals hemispheric climate dynamics (Southern CA, USA): Palaeogeography, Palaeoclimatology, Palaeoecology, v. 241, no. 2, p. 267-283.

Pazzaglia, F. J., Gardner, T. W., and Merrits, D. J., 1998, Bedrock fluvial incision and longitudinal profile development over geologic time scales determined by fluvial terraces: Geophysical Monograph, v. 107, p. 207-235.

Pazzaglia, F. J., and Brandon, M. T., 2001, A fluvial record of long-term steady-state uplift and erosion across the Cascadia forearc high, western Washington State: American Journal of Science, v. 301, no. 4-5, p. 385-431.
Proffett, J. M., Jr., 1977, Cenozoic geology of the Yerington District, Nevada, and implications for the nature and origin of Basin and Range faulting: Geological Society of America Bulletin, v. 88, no. 2, p. 247-266.
Quade, J., Forester, R. M., and Whelan, J. F., 2003, Late Quaternary paleohydrologic and paleotemperature change in southern Nevada: Special Paper - Geological Society of America, v. 368, p. 165-188.
Ritter, D. F., 1967, Terrace development along the front of the Beartooth Mountains, southern Montana: Geological Society of America Bulletin, v. 78, no. 4, p. 467-483.
Ruff, R., Shlemaon, R.J., 1991, Character and recency of faulting along a portion of the northern Springville fault, Camarill, Ventura County, California *in* Blake, T. F., ed., Engineering Geology along the Simi-Santa Roas fault sytem and adjacent areas, Simi Valley to Camarillo, Ventura, California, p. 147.
Schwartz, D. P., Coppersmith, K. J., and Anonymous, 1984, Fault behavior and characteristic earthquakes; examples from the Wasatch and San Andreas fault zones, Journal of Geophysical Research: Washington, American Geophysical Union, p. 5681-5698.
Shaw, J. H., and Suppe, J., 1996, Earthquake hazards of active blind-thrust faults under the central Los Angeles Basin, California: Journal of Geophysical Research, B, Solid Earth and Planets, v. 101, no. 4, p. 8623-8642.
Sorlien, C. C., Kamerling, M. J., Seeber, L., and Broderick, K. G., 2006, Restraining segments and reactivation of the Santa Monica-Dume-Malibu Coast fault system, offshore Los Angeles, California: Journal of Geophysical Research-Solid Earth, v. 111, no. B11, p. -.
Stolar, D. B., Willett, S. D., & Montgomery, D. R. (2007). Characterization of topographic steady state in Taiwan. *Earth and Planetary Science Letters,* vol.261*,* no.3-4, p. 421-431.
Strahler, A. N., 1952, Hypsometric (area-altitude curve) analysis of erosional topography: Geological Society of America Bulletin, v. 63, no. 11, p. 1117-1141.
Tierra Tech Testing Laboratory, 1978, Geologic reports for Tract 2910 and Tract 2930, eastern Camarillo (unpublished report).
Treiman, J. A., 1997, Springville, Camarillo and related faults in the Camarillo and Santa Paula Quadrangles, Ventura County, California, Division of Mines and Geology, Fault Evaluation Report FER-237 (unpublished).
Treiman, J. A., 1998, Simi-Santa Rosa fault zone in the Moorpark, Newbury Park, Simi Valley East, Simi Valley west, Thousand Oaks quadrangles, Ventura County, California, Division of Mines and Geology, Fault Evaluation Report FER-244 (unpublished).
Twiss, R. J., and Moores, E. M., 1992, Structural geology.

U.S. Geological Survey and Southern California Earthquake Scientists (USGS and SCEC), 1994, The magnitude 6.7 Northridge California, earthquake of 17 January 1994: Science, vol. 266, p. 389-397.
Vail, P. R., and Mitchum, R. M., Jr., 1977, Seismic stratigraphy and global changes of sea level; Part 1, Overview.
Walcott, R. C., and Summerfield, M. A., 2008, Scale dependence of hypsometric integrals: An analysis of southeast African basins: Geomorphology, v. 96, no. 1-2, p. 174-186.
Walls, C., Rockwell, T., Mueller, K., Bock, Y., Williams, S., Panner, J., Dolan, J., and Fang, P., 1998, Escape tectonics in the Los Angeles metropolitan region and implications for seismic risk: Nature, v. 394, no. 6691, p. 356-360.
Wagner, H. M. L., E.B., Roeder, M.A., Prothero, D.R., McDaniel, G. E. J., 2007, A new Irvingtonian land mammal assemblage from the Saugus Formation, Moorpark, Ventura County, California: Bulletin - Southern California Academy of Sciences, v. 106, no. 2, p. 141.
Weigand, P. W., Savage, K. L., and Nicholson, C., 2002, The Conejo Volcanics and other Miocene volcanic suites in southwestern California: Special Paper - Geological Society of America, v. 365, p. 187-204.
Wells, S. G., Brown, W. J., Enzel, Y., Anderson, R. Y., and McFadden, L. D., 2003, Late Quaternary geology and paleohydrology of pluvial Lake Mojave, Southern California: Special Paper - Geological Society of America, v. 368, p. 79-114.
Whitney, R. A., Gath, E.M., 1991, Structure, tectonics, and surface rupture hazard at the Las Posas anticlne, Ventura County, California, *in* Blake, T. F., ed., Engineering Geology along the Simi-Santa Rosa fault system and adjacent areas, Simi Valley to Camarillo, Ventura, California, p. 164.
Williams, R. E., 1983, Miocene volcanism in the central Conejo Hills and western Simi Valley, Ventura, California, *in* Cenozoic geology of the Simi Valley area, Southern California, *eds*., Squires, R. L. and Folewicz, M. V., Society of Economic Paleoentolgists and Mineralologists., Pacific Section, Los Angeles, CA., p. 183-190.
Wright, T. L., 1991, Structural geology and tectonic evolution of the Los Angeles basin, California, *in* Biddle, K.T., ed., Active margins basins:American Association of Petroleum Geologist Memoir 52, p. 35-135.
Yeats, R. S., 1988, Late Quaternary Slip Rate on the Oak Ridge Fault, Transverse-Ranges, California - Implications for Seismic Risk: Journal of Geophysical Research-Solid Earth and Planets, v. 93, no. B10, p. 12137-12149.
Yeats, R. S., Huftile, G. J., and Stitt, L. T., 1994, Late Cenozoic Tectonics of the East Ventura Basin, Transverse Ranges, California: AAPG Bulletin-American Association of Petroleum Geologists, v. 78, no. 7, p. 1040-1074.
Yerkes, R. F., Sarna-Wojcicki, A. M., and Lajoie, K. R., 1987, Geology and Quaternary deformation of the Ventura area, scale 1:24,000.

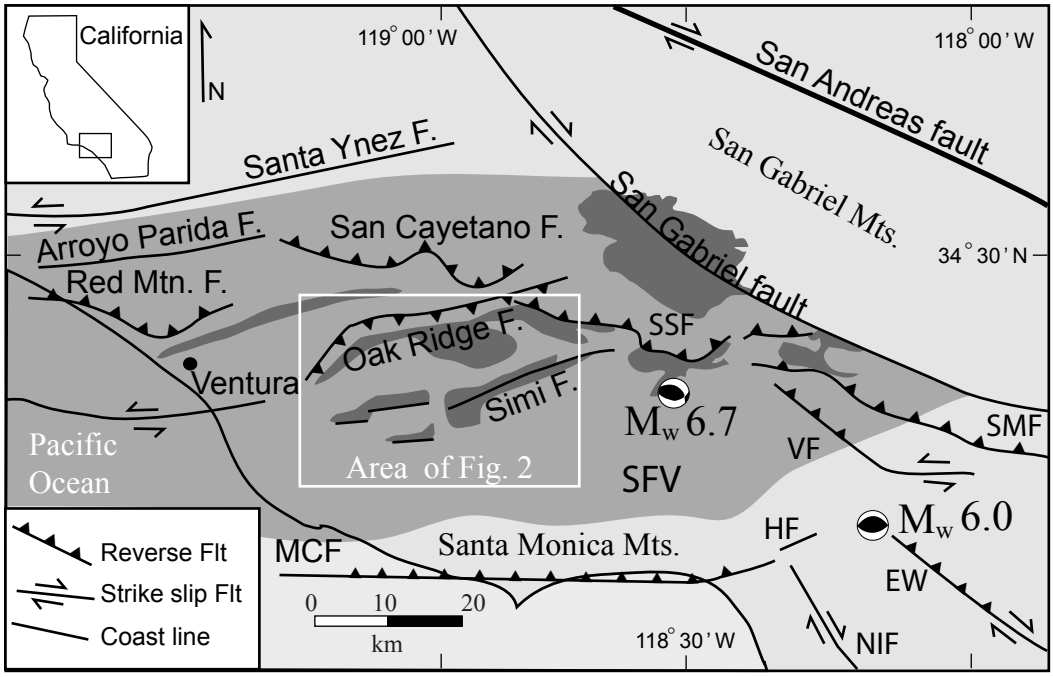

Figure 1.
Simplified index map of the principle active faults in southern California with respect to the study area (white box). The study area lies in the hangingwall of the south-dipping Oak Ridge fault and the north-dipping Malibu Coast fault. Large gray shaded area shows the location of the Mio-Pliocene Ventura basin. Darker gray patches show the approximate distribution of Plio-Pleistocene Saugus Formation. Focal mechanisms show the approximate hypocenter locations for the 1987 Mw6.0 Whittier Narrows and 1994 Mw6.7 Northridge earthquakes (lower hemisphere projections). SSF-Santa Susana Fault; VF-Verdugo Fault; NIF-Newport-Inglewood Fault; EW-Elsinore/Whittier Fault; SFV-San Fernando Valley; SMF- Sierra Madre fault.

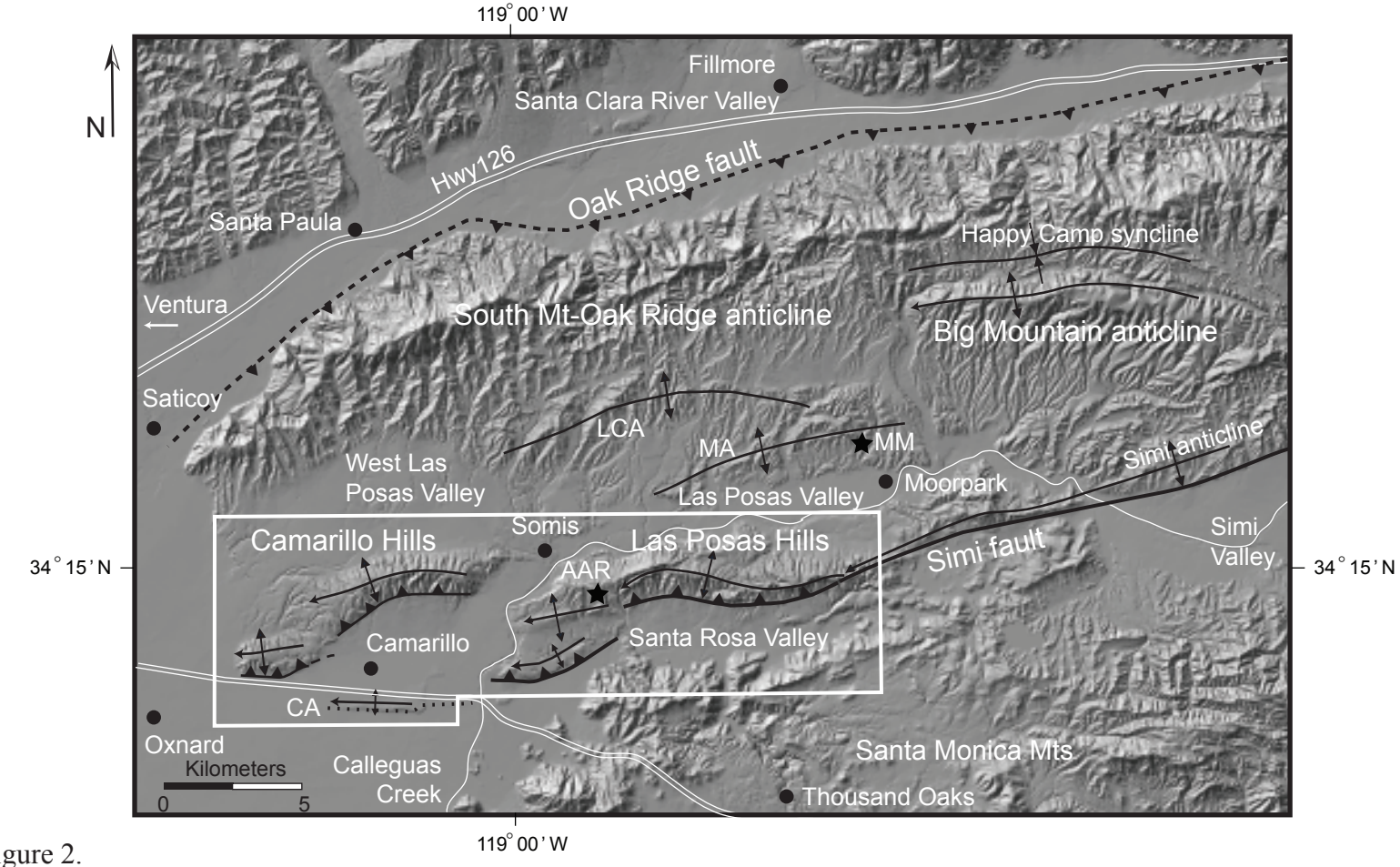

Figure 2.

Shaded relief map illustrating the dominant east-west structural grain of this part of the Western Transverse Ranges and showing the important faults and folds that accommodate north-south contraction within the CFB. The white box shows the area of the CFB and the approximate location of Figures 6 and 12a. AAR-Amino Acid Racemization age date; CA-Camarillo Anticline; MM-Moorpark Mammoth site; LCA-Long Canyon anticline; MA-Moorpark anticline.

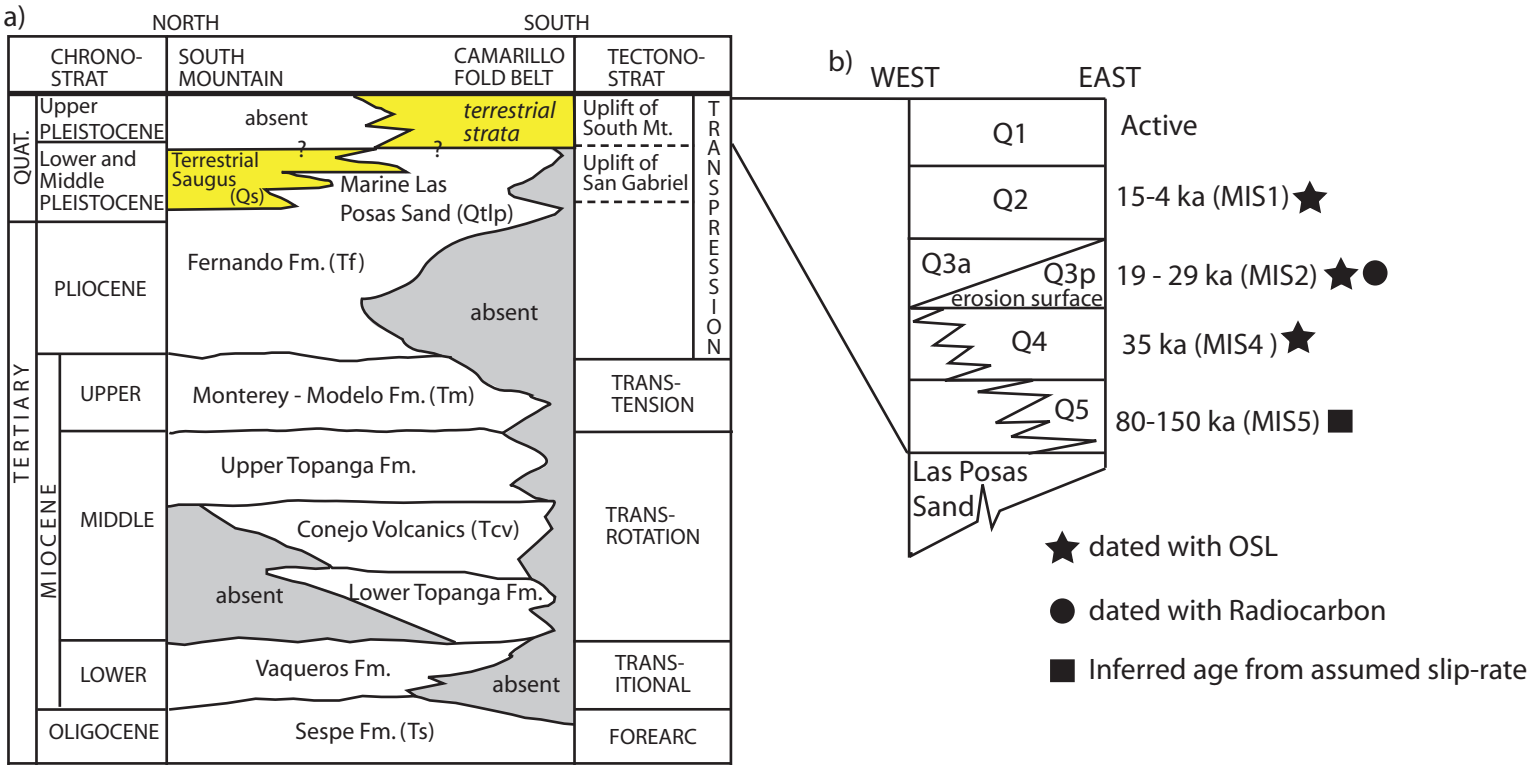

Figure 3.

Stratigraphic column of Oligocene to Holocene strata in the Western Transverse Ranges (Modified from Ingersoll, 2001). a) Column illustrating the north to south stratigraphic variability between South Mountain to the north and the CFB to the south. Plio-Pleistocene formations in the CFB unconformably overlie Oligocene to Miocene strata. The Pliocene Fernando Fm. is absent in the CFB. b) Column illustrating the west to east stratigraphic variability of Upper - Middle Pleistocene to Holocene sediments in the CFB and the nomenclature used for this study. Q5 and Q4 likely characterize a time-transgressive westward younging progradational sequence of terrestrial strata. Q3a and sediments that overlie the Q3p are coeval and are lateral equivalents with Q3a deposition occurring to the west in a more distal environment than sediments deposited on the Q3p erosion surface.

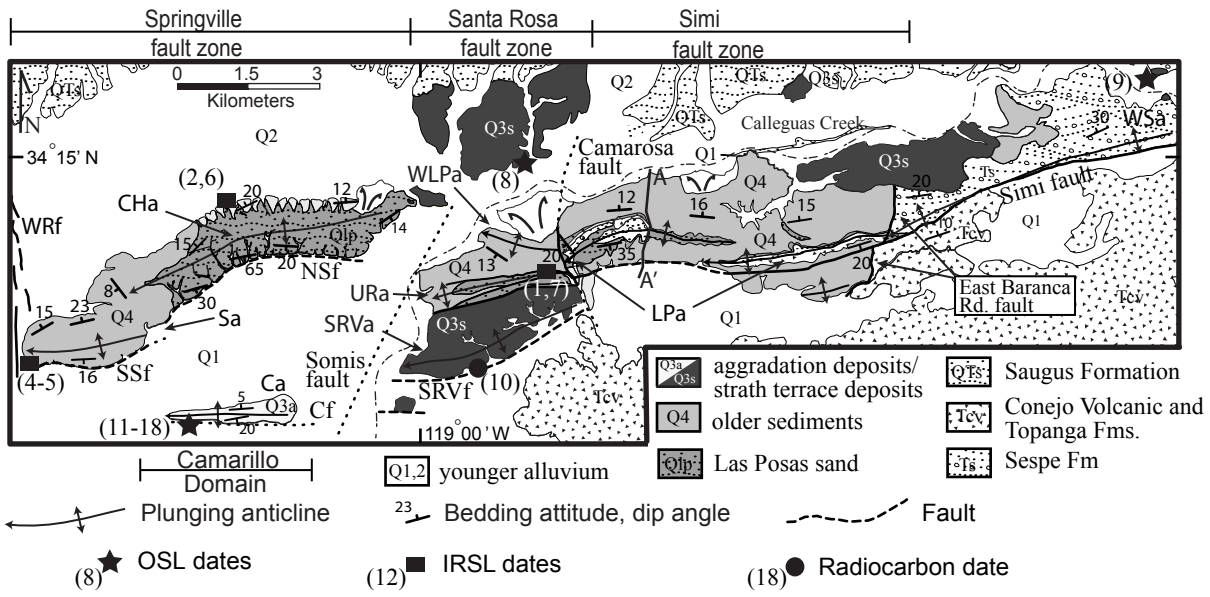

Figure 4. Generalized geologic map of the CFB. Numbers adjacent sample sites corelate to numerical dates shown on Table 1. Approximate locations of discrete structural domains delimited by north-striking cross faults are shown above and bellow the map. Ca- Camarillo anticline; Cf- Camarillo fault; CHa-Camarillo Hills anticline; LPa- Las Posas anticline; SRVa-Santa Rosa Valley anticline; SRVF=Santa Rosa Valley fault; SSf- Southern Springville fault; URa- Upland Road anticline; WRf- Wright Road fault; WLPa- Western Las Posas anticline; WSa-Western Simi anticline

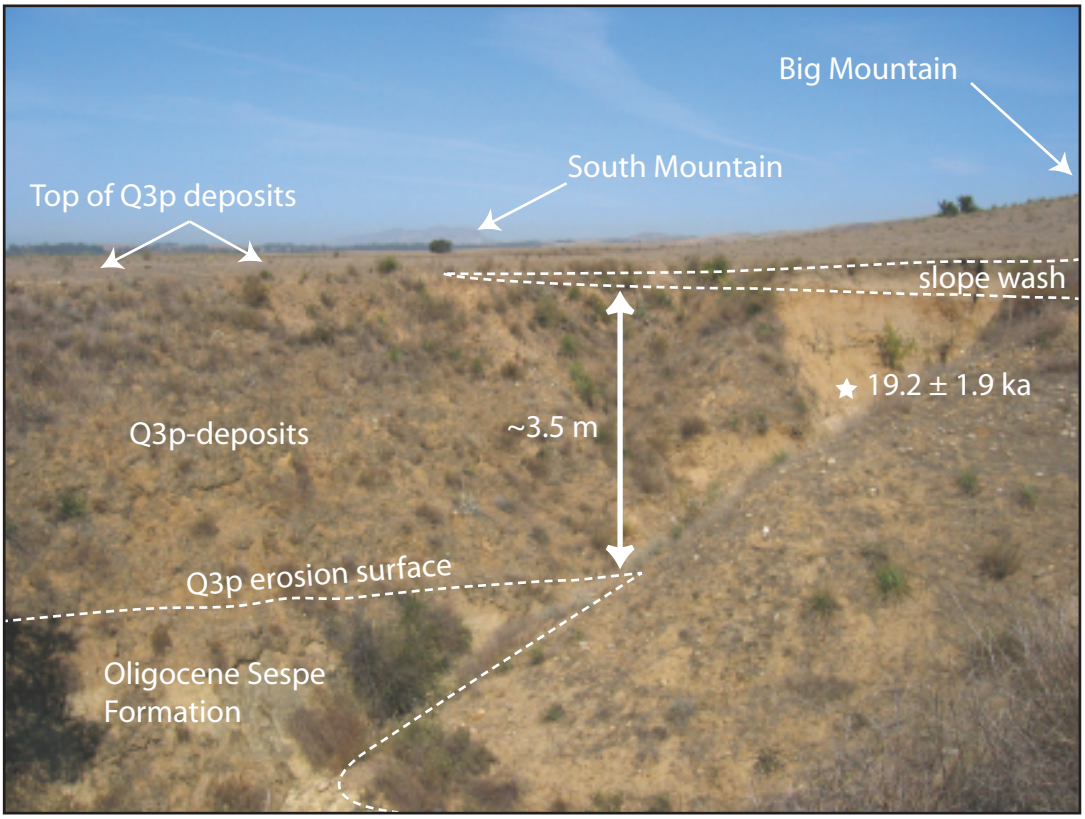

Figure 5.
Photograph of Q3p sediment overlying regional erosion surface cut on Sespe Formation (view to the west). Q3p deposits are commonly stripped exposing the near planar bedrock erosion surface. Where present sediment thicknesses range between 2 - 3.5 m and are composed of cross bedded sand and poorly sorted cobble lag deposits. See figure 2 for location of sample 18OSL07 and this photograph.

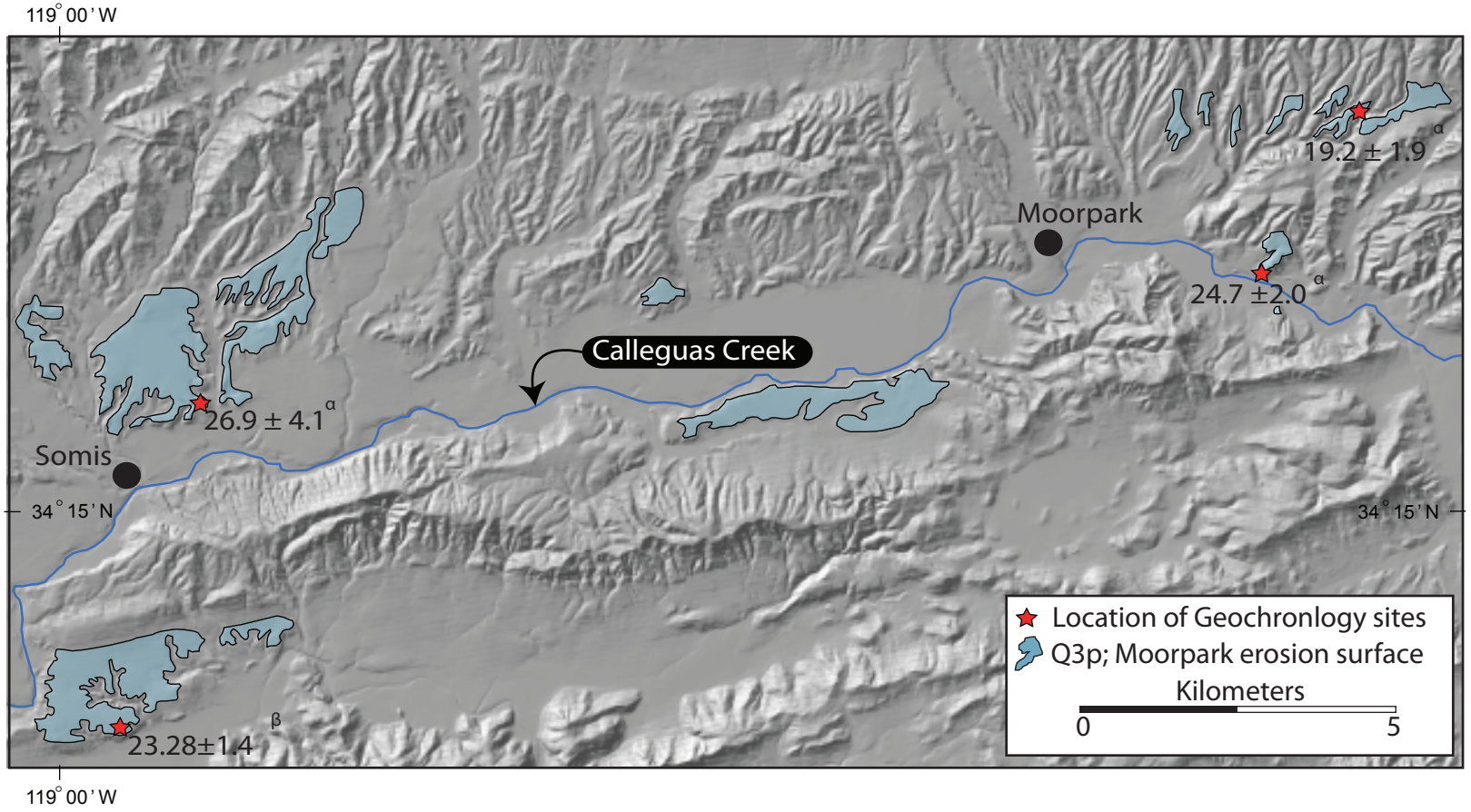

α Optical Stimulated Luminescence (OSL) age date (DeVecchio et al., in prep)

β Radiocarbon age date (Blake, 1991)

Figure 6.
Lateral extent of the Q3p Moorpark erosion surface. The surface is cut onto Oligocene Sespe, Pleistocene Saugus, and upper Pleistocene Q4 deposits (this study).

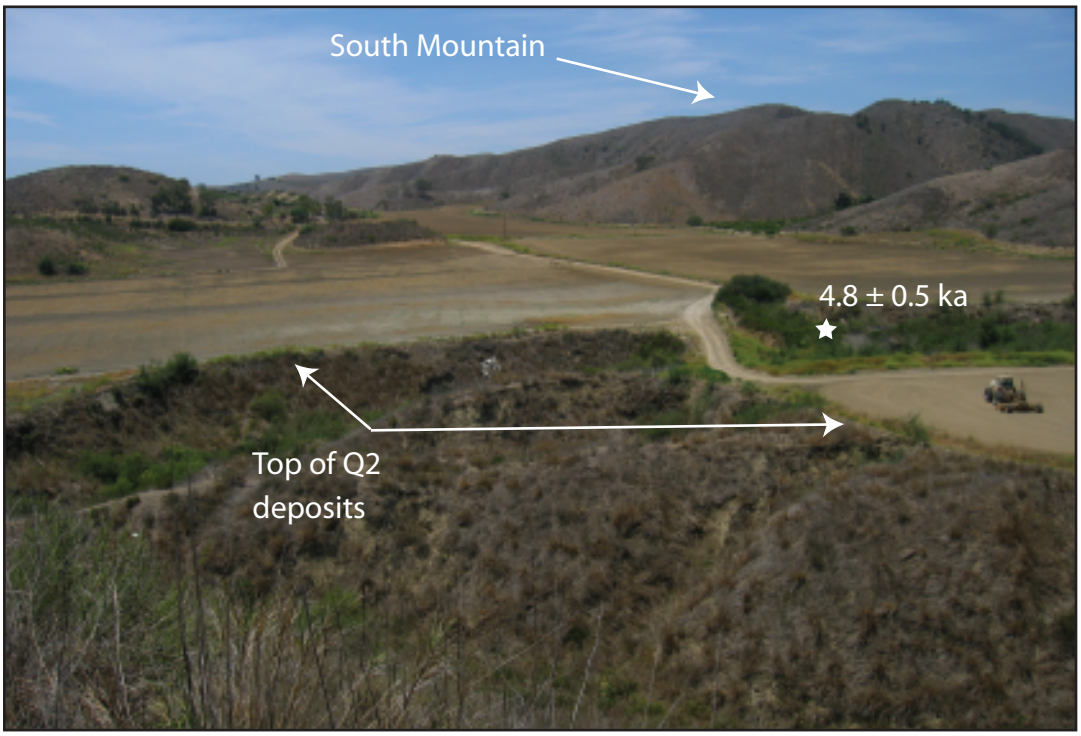

Figure 10
Photograph of the Q2 deposits on the south flank of South Mountain (view to the north). Note the broad flat valley floor composed of Q2 deposits that locally extend from the west Las Posas valley to the south to near the topographic highs of South Mountain. Q2 deposits fill topographic and structural lows north of the CFB and are locally >20 m in thickness. See figure 4 for location of sample site 19OSL07 this photograph.

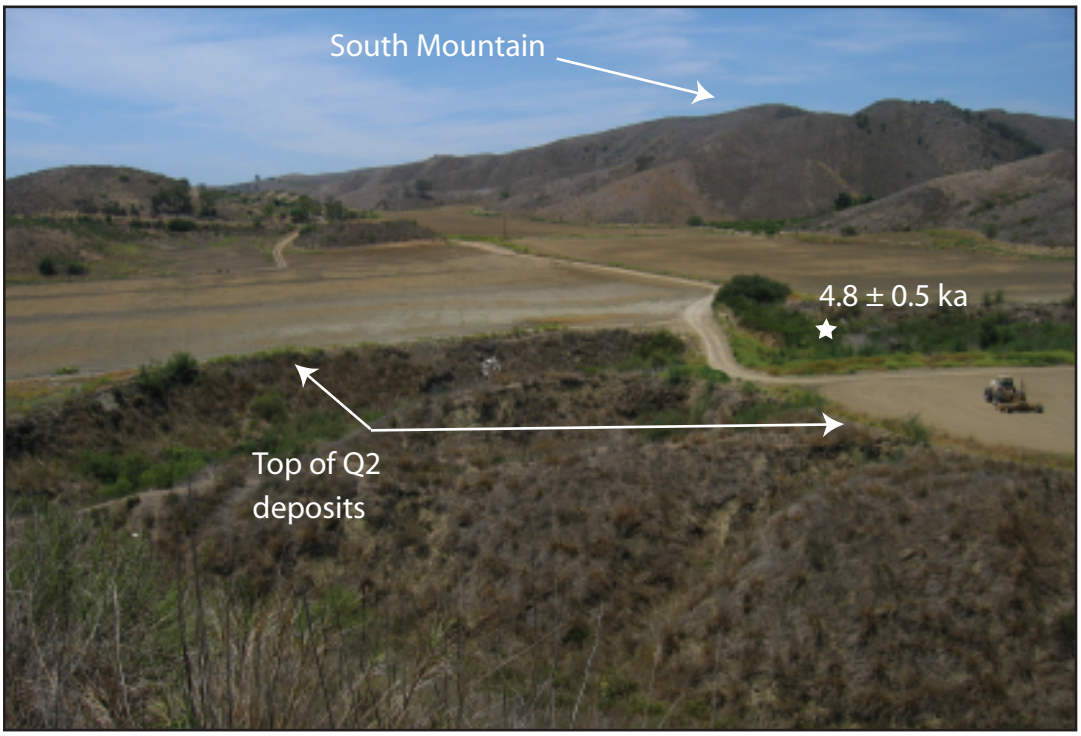

Figure 7
Photograph of the Q2 deposits on the south flank of South Mountain (view to the north). Note the broad flat valley floor composed of Q2 deposits that locally extend from the west Las Posas valley to the south to near the topographic highs of South Mountain. Q2 deposits fill topographic and structural lows north of the CFB and are locally >20 m in thickness. See figure 4 for location of sample site 19OSL07 this photograph.

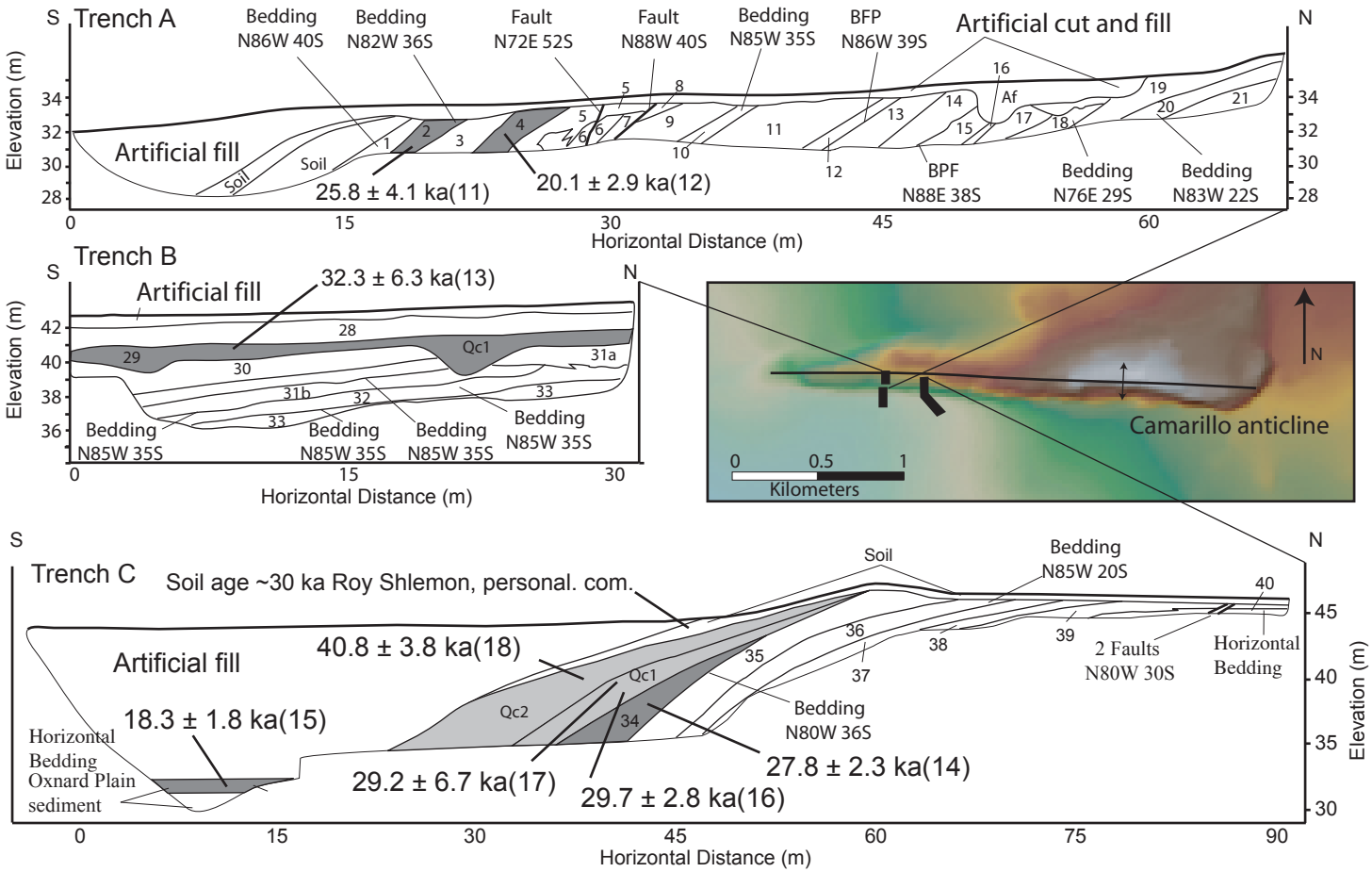

Figure 8.
Schematic line drawings of trench logs across the Camarillo anticline. Inset shows shaded relief map showing the relative position of fault trenches with respect to the axis and topographic expression of the Camarillo anticline. See Figure 2 for location of the Camarillo anticline. Numbered units (1-40) are an interbedded sequence of well-sorted fluvial conglomerate, sandstone, and siltstone beds referred to as Saugus Formation in consultant logs (Q3a this study). Dark grey numbered fluvial strata were sampled for OSL dating. Interpreted colluvial units (Qc 1 and 2) are locally discordant with the underlying fluvial strata and are interpreted to record post-tectonic deposition on a growing fold. Light-gray shaded units reflect Quaternary colluvial packages sampled for OSL dating. Trenches A and B expose several south-dipping faults interpreted as back-thrusts or bending moment normal faults. The Camarillo fault was not distinctly encountered in any of the trenches. Deformation along the Camarillo fault zone is best characterized by blind faulting. Age dates are from OSL analysis with numbers in parentheses corresponding sample numbers in Table 1. Note Trench C is not the same scale as trenches 1 and 2.

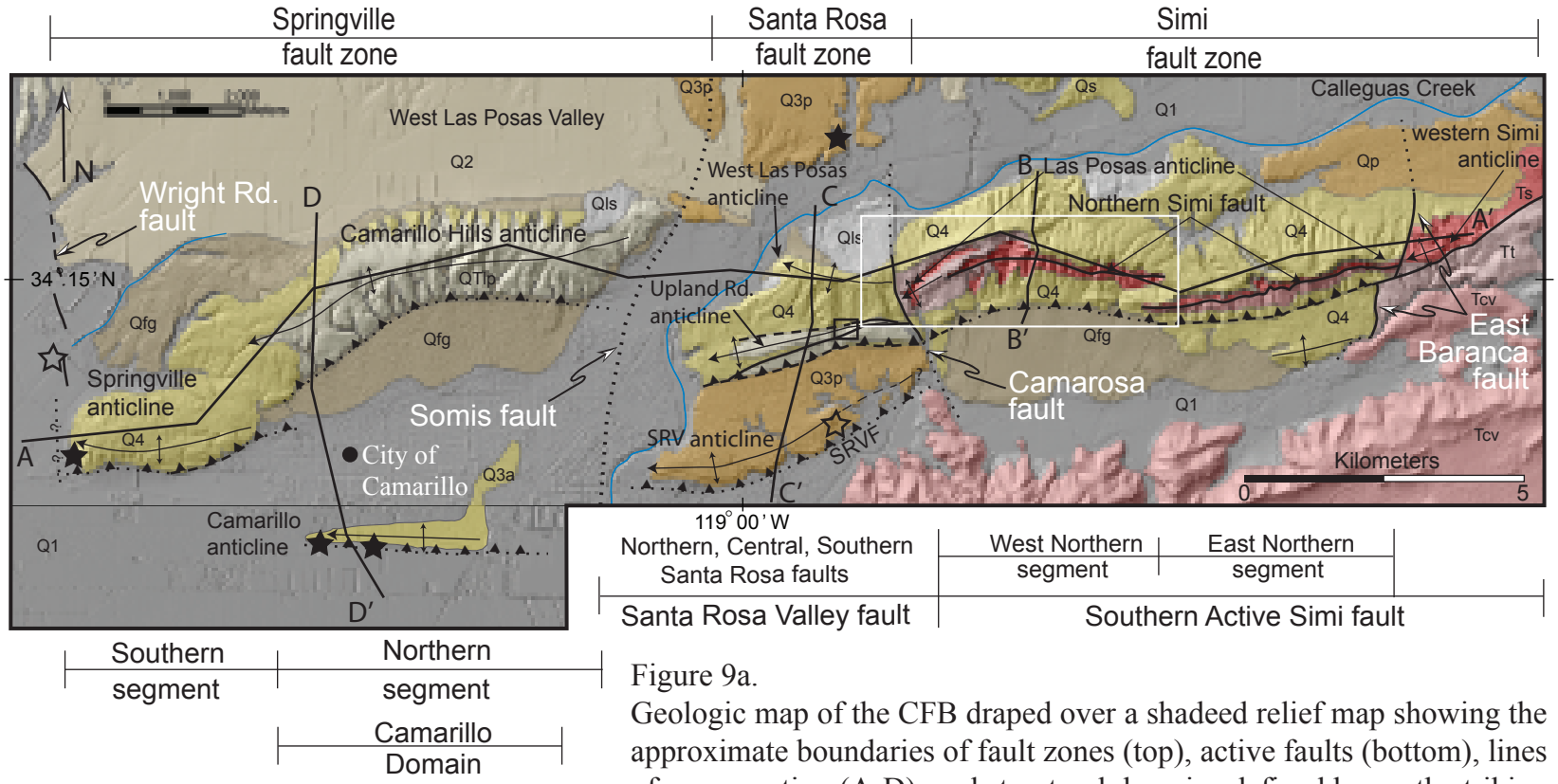

Figure 9a.
Geologic map of the CFB draped over a shadeed relief map showing the approximate boundaries of fault zones (top), active faults (bottom), lines of cross-section (A-D), and structural domains defined by north-striking transverse faults. Note, most transverse faults are unbroken by east-trending faults and characterized by changes in the orientation, geometry and number of structures across these boundaries, with the exception of the East Baranca fault, which is cut be the southern splay of the Simi fault. Area of figure 14 shown by white box. OSL age-solid stars, Radio-carbon age-open star, AAR age date-open square, SRVF - Santa Rosa Valley fault. See figure 4 for geologic unit abbreviations.

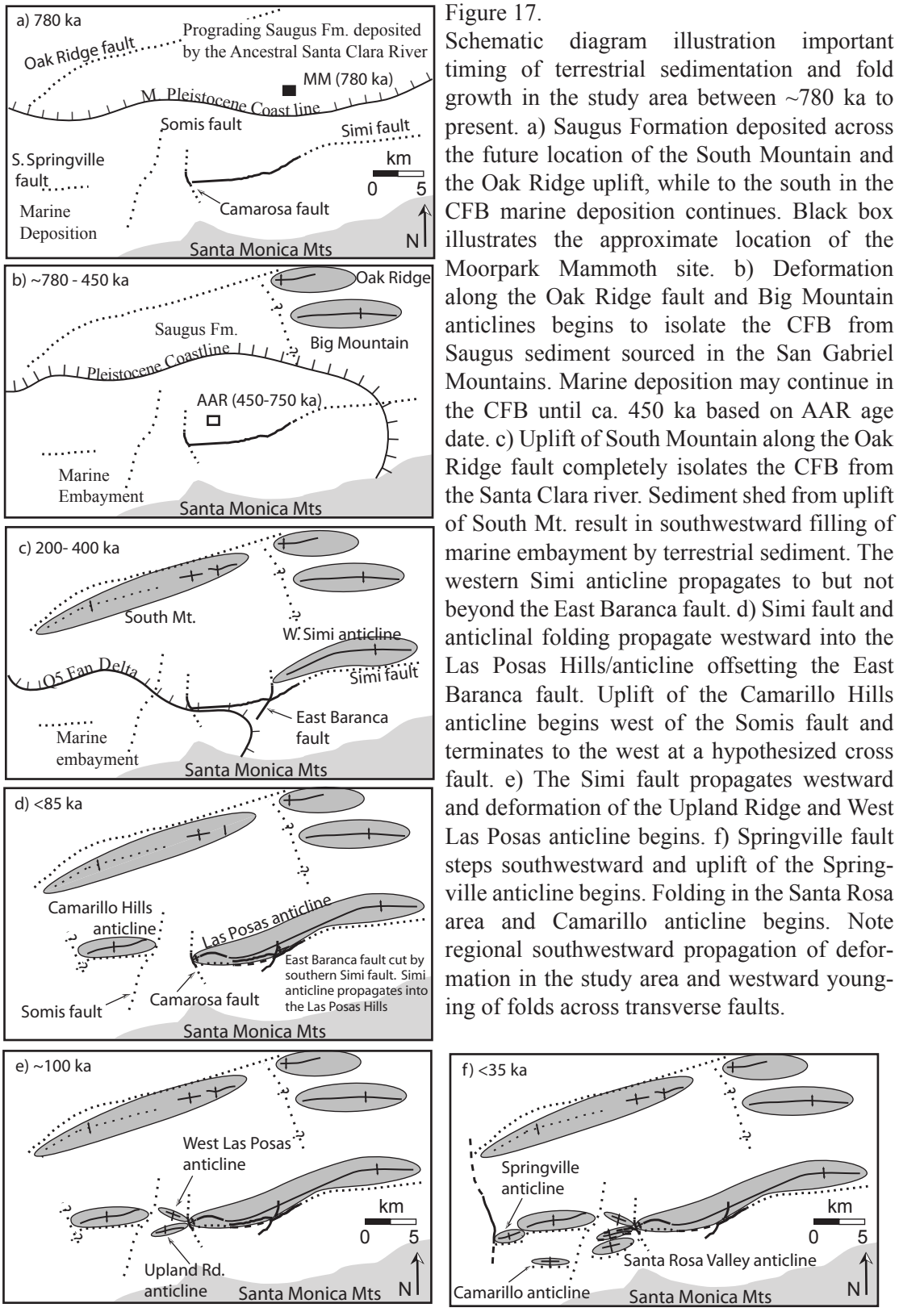

Figure 17.
Schematic diagram illustration important timing of terrestrial sedimentation and fold growth in the study area between ~780 ka to present. a) Saugus Formation deposited across the future location of the South Mountain and the Oak Ridge uplift, while to the south in the CFB marine deposition continues. Black box illustrates the approximate location of the Moorpark Mammoth site. b) Deformation along the Oak Ridge fault and Big Mountain anticlines begins to isolate the CFB from Saugus sediment sourced in the San Gabriel Mountains. Marine deposition may continue in the CFB until ca. 450 ka based on AAR age date. c) Uplift of South Mountain along the Oak Ridge fault completely isolates the CFB from the Santa Clara river. Sediment shed from uplift of South Mt. result in southwestward filling of marine embayment by terrestrial sediment. The western Simi anticline propagates to but not beyond the East Baranca fault. d) Simi fault and anticlinal folding propagate westward into the Las Posas Hills/anticline offsetting the East Baranca fault. Uplift of the Camarillo Hills anticline begins west of the Somis fault and terminates to the west at a hypothesized cross fault. e) The Simi fault propagates westward and deformation of the Upland Ridge and West Las Posas anticline begins. f) Springville fault steps southwestward and uplift of the Springville anticline begins. Folding in the Santa Rosa area and Camarillo anticline begins. Note regional southwestward propagation of deformation in the study area and westward younging of folds across transverse faults.

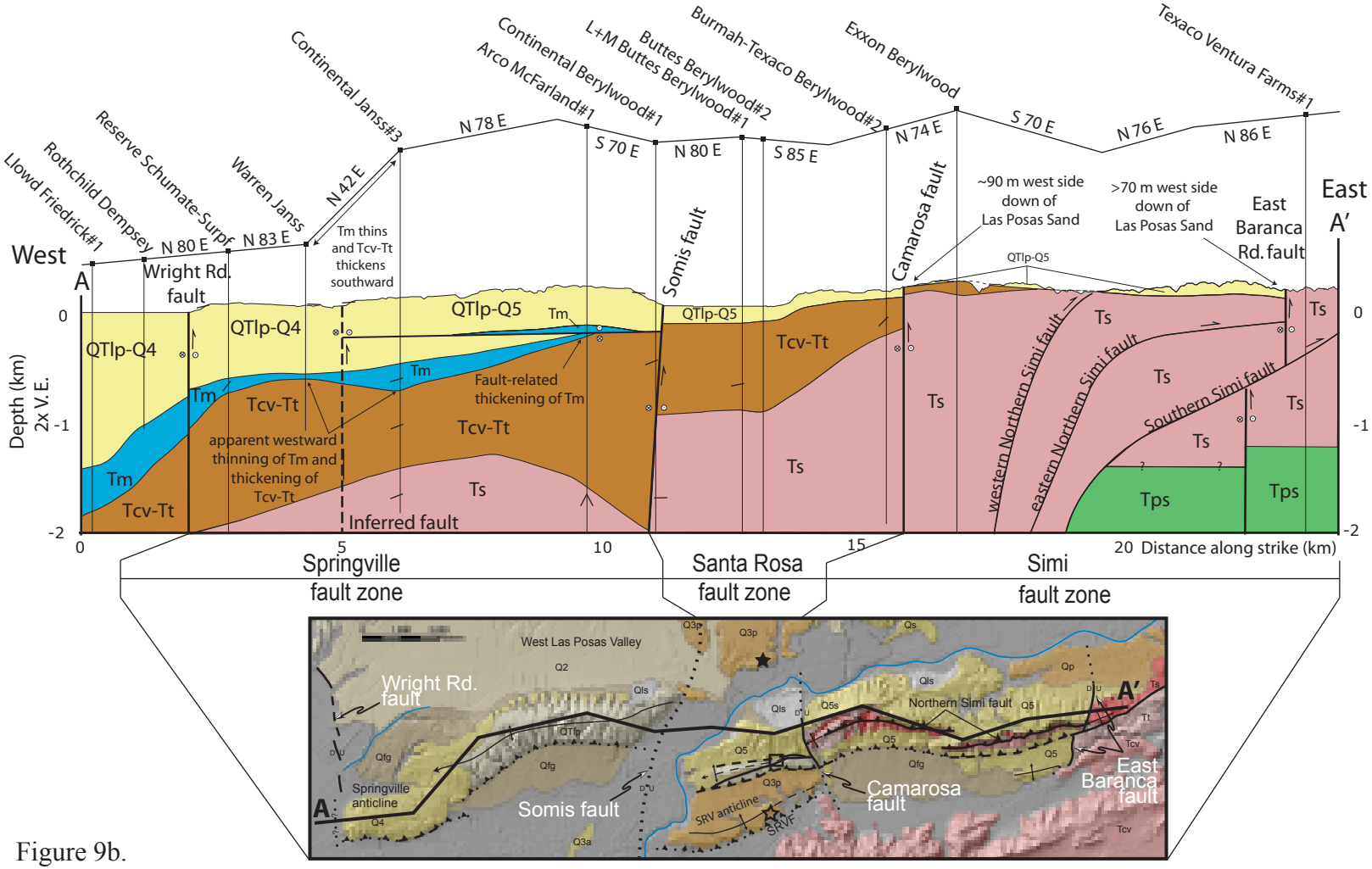

Figure 9b.

Cross section A-A'. Names and well locations along the cross-section line are shown across the top. Note westward decrease in structural relief. Dip angles appear steeper due to 2x vertical exaggeration. See figure 4 for geologic unit abbreviations.

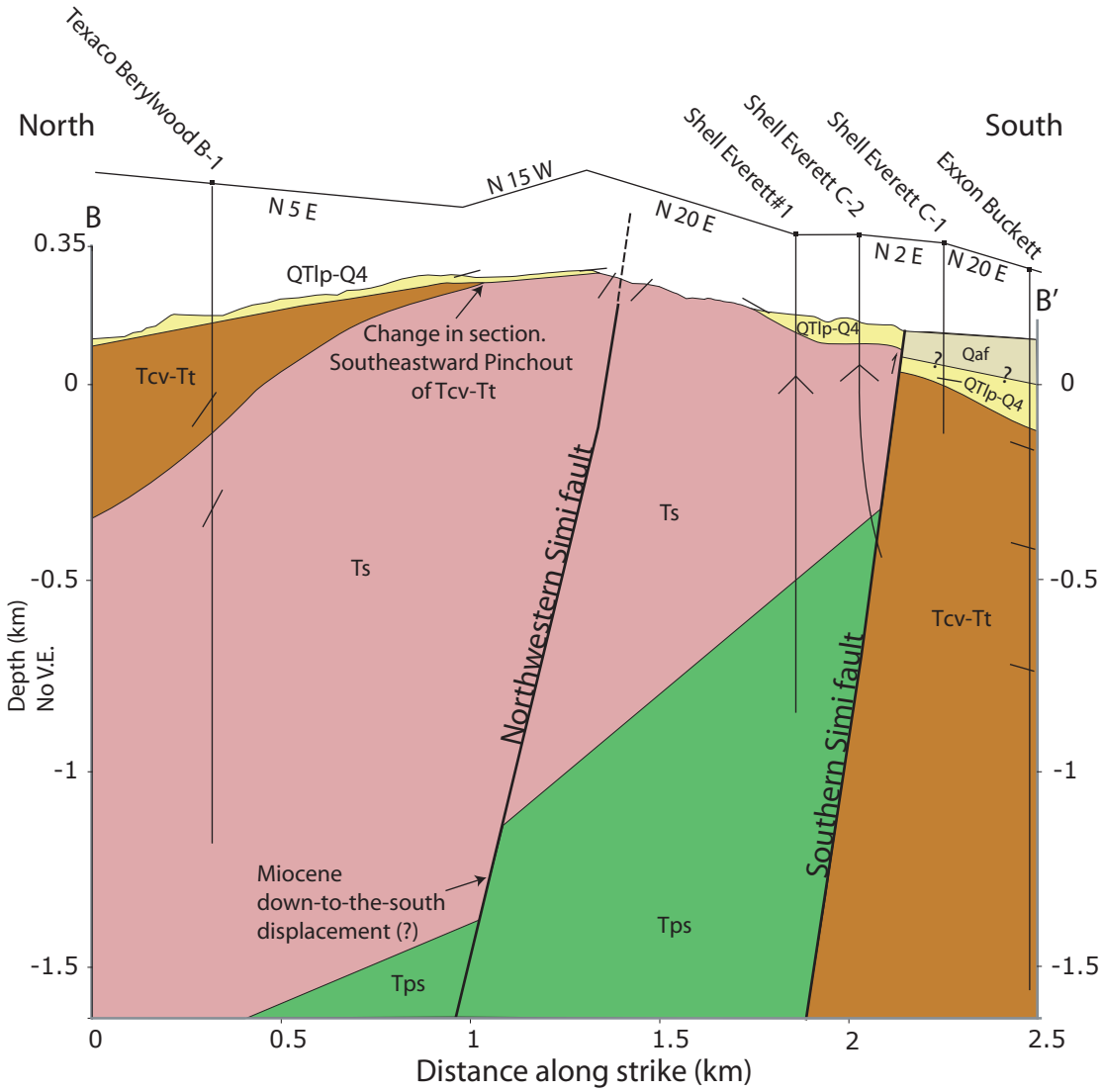

Figure 10.
Cross section B-B' across the NW and southern Simi fault splays. Note thick section of Tcv-Tt south of the southern splay of the Simi fault indicating Miocene down-to-the south displacement. Note cutoff angles between the southern Simi fault and Miocene strata are ~90 degrees. Location of cross section shown on Figure 9a. Well names shown across the top. See figure 4 for geologic unit abbreviations.

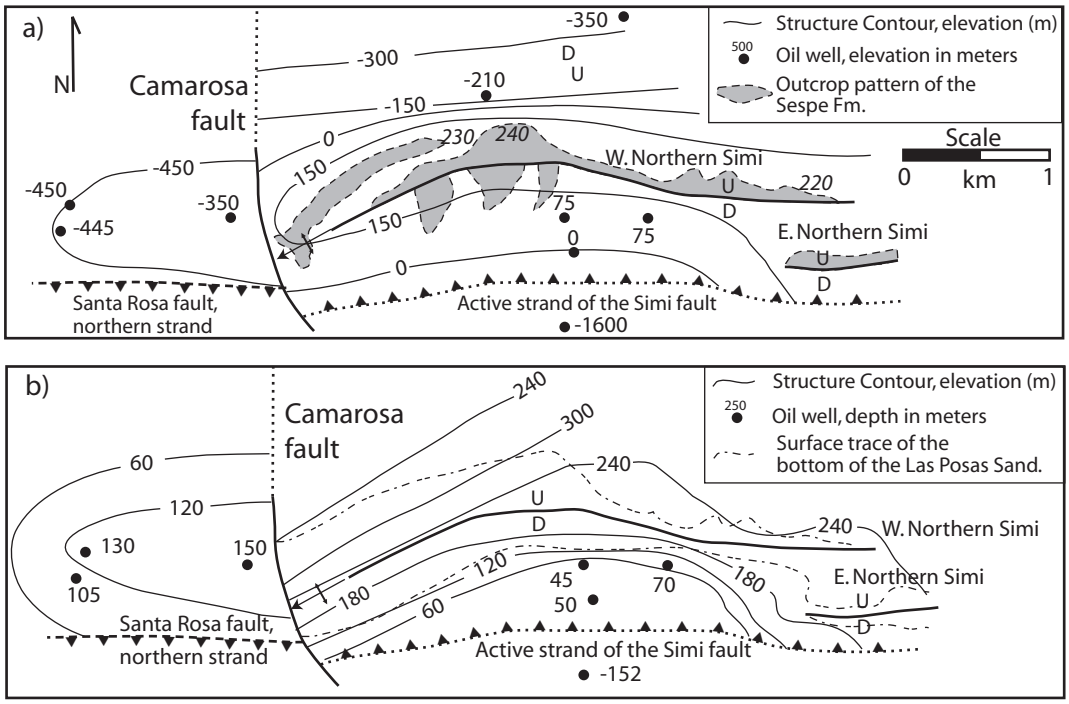

Figure 11.
Structure contour maps adjacent the Camarosa and southern Simi faults. a) Contour map showing the top of the Oligocene Sespe Formation. Note the top of the Sespe Formation is 500 m lower west of the Camarosa fault and 1600 m lower south of the southern strand of the Simi fault. Downward displacement of the top of the Sespe Formation is interpreted to reflect tectonic lowering due to Miocene transrotational deformation. b) Contour map of the top of the Pleistocene Las Posas Sand. Note 90 m of uplift of the base of the Pleistocene strata east of the Camarosa fault and 200 m of uplift north of the southern Simi fault. Uplift is interpreted to be the result of Quaternary transpressional deformation.

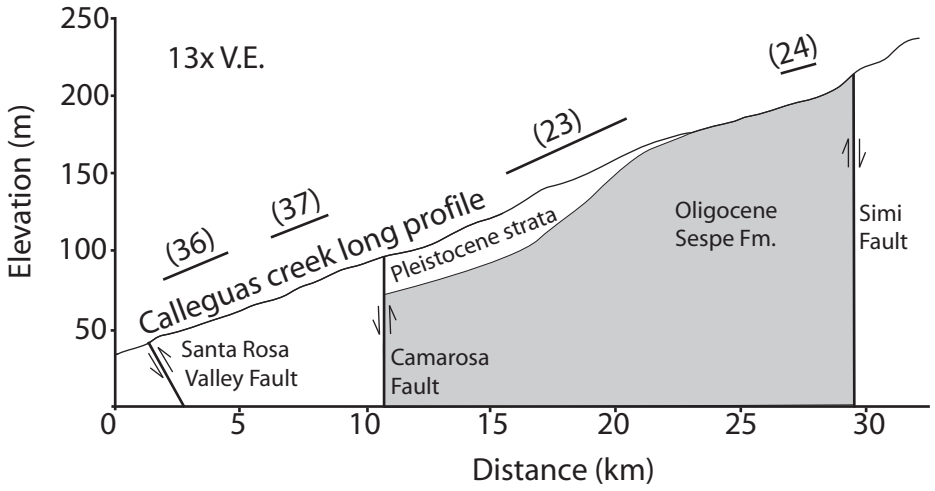

Figure 12.
Long profile of Calleguas Creek with respect to the Q3p surface. The elevational difference between Calleguas Creek and the Q3p surface is in meters and shown in parentheses above the approximate location of the pediment surface with respect to the long profile. After crossing the approximate location of the Camarosa fault, spacing between the two datum increases by ~13 m, which suggests an increase in post-23 ka uplift west of the fault.

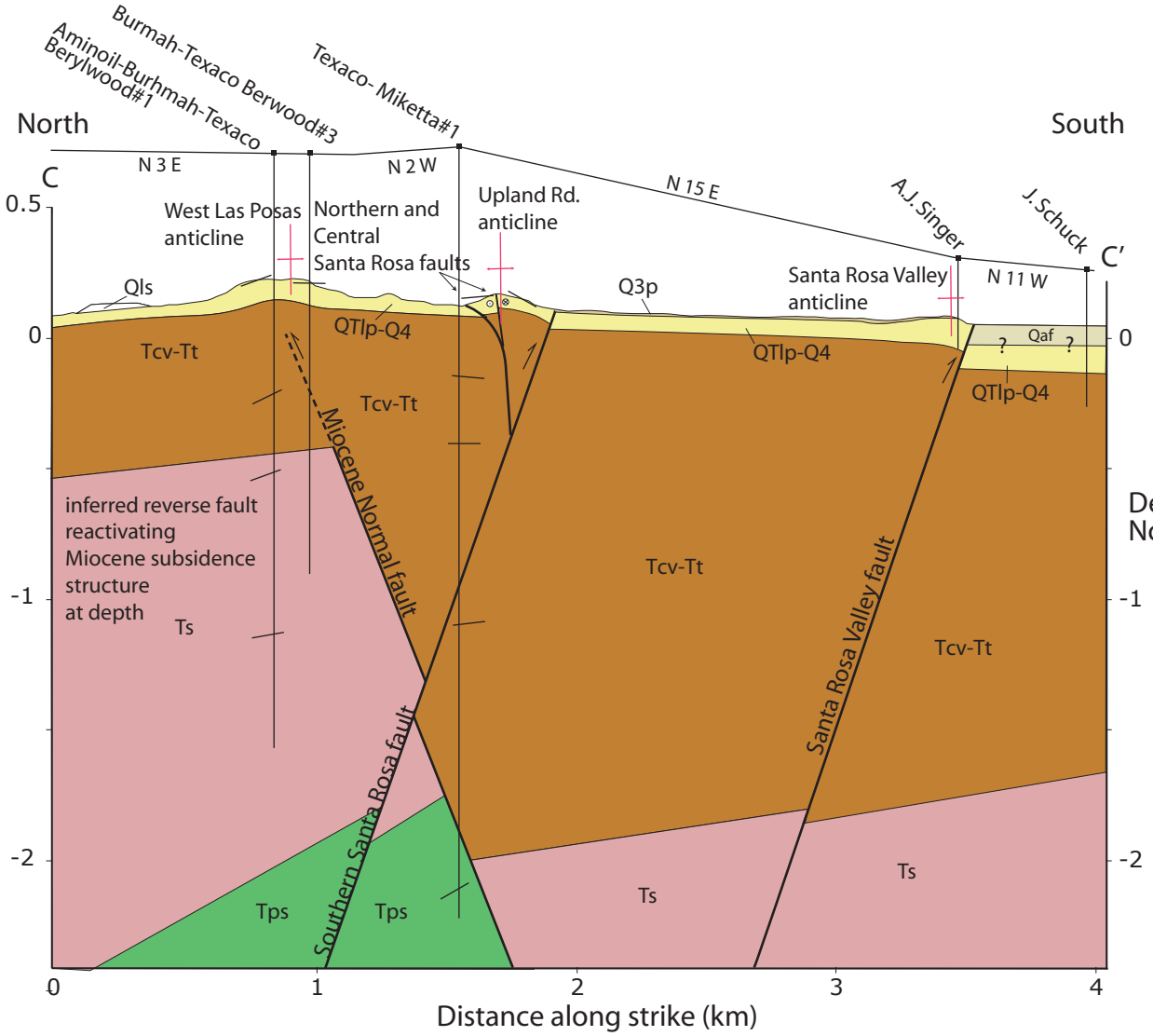

Figure 13.
Cross section C-C' across the NW across the Santa Rosa Domain. Note thickening of QTlp-Qs south of the southern Santa Rosa fault. Location of cross section shown on Figure 10. Well names shown across the top. See figure 4 for geologic unit abbreviations.

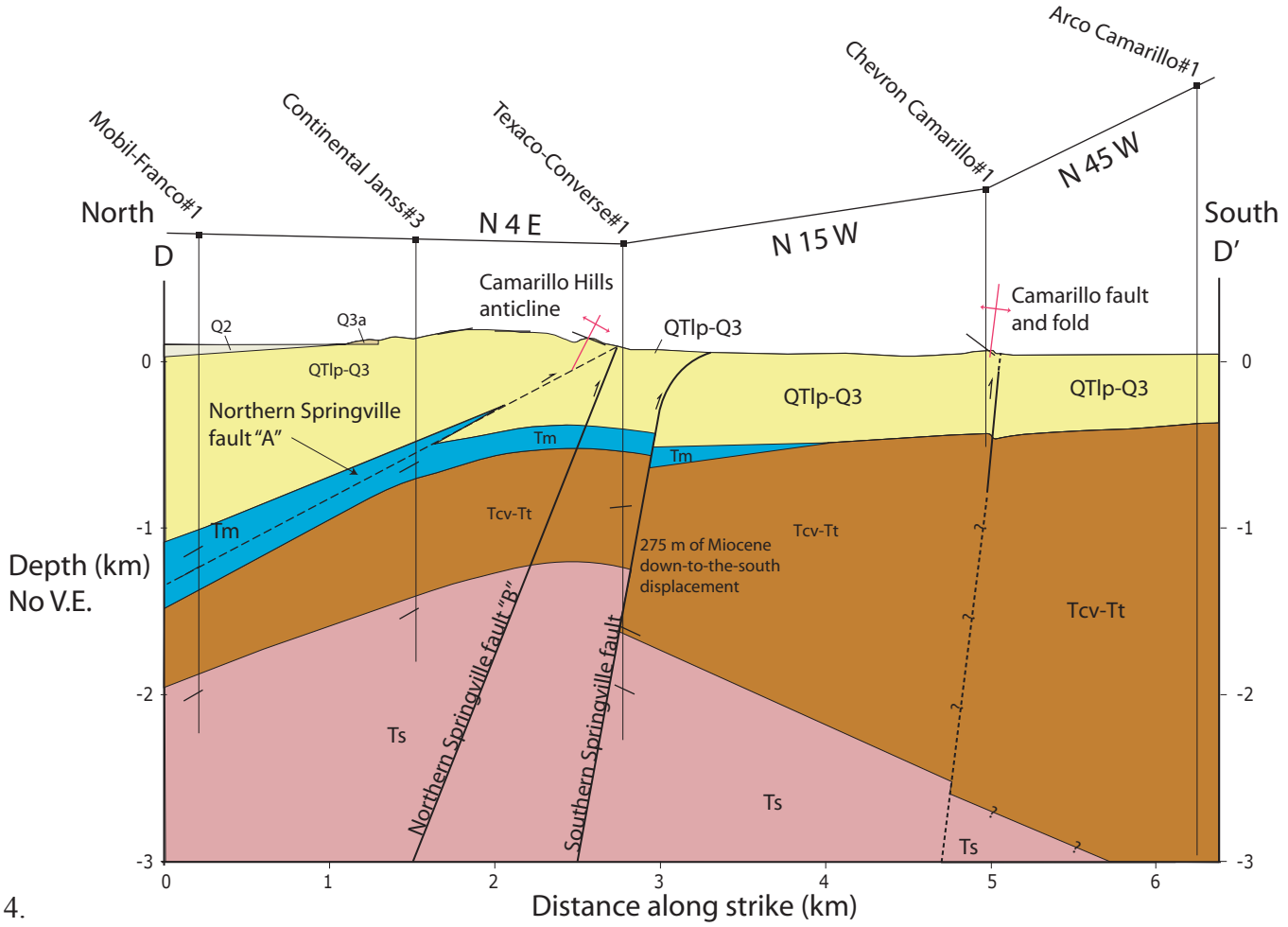

Figure 14.
Cross section D-D' across the Springville and Camarillo fault zones. Note 275 m of down-to the south Miocene displacement of the top of the Sespe Formation, southward thickening of Tcv-Tt. Two fault plane solutions are shown for the northern Springville fault. Solution A dips ~25° and Solution B dips ~75°. See figure 4 for geologic unit abbreviations.

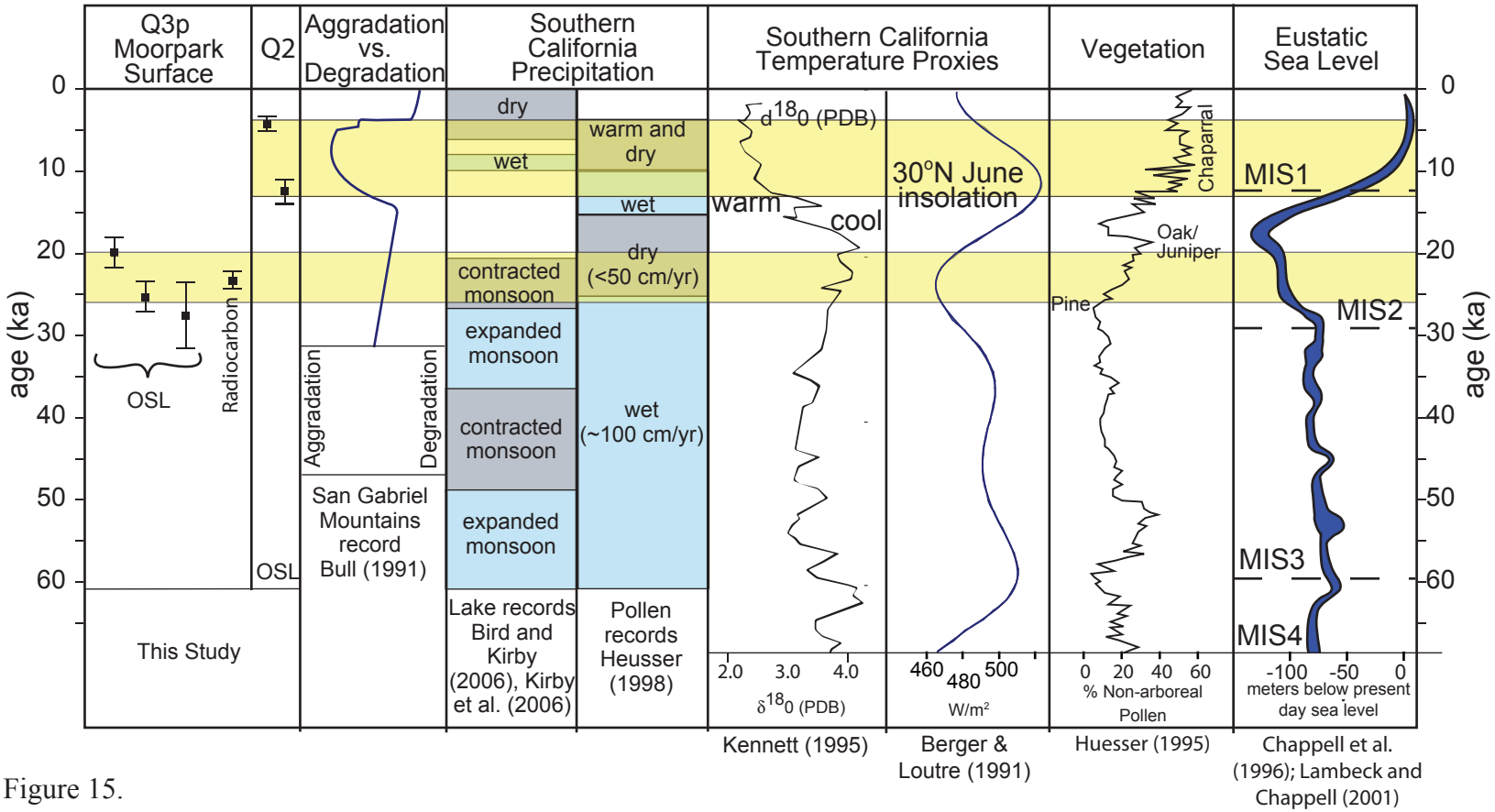

Figure 15.
Correlation chart showing the relationship between bedrock planation of the Q3p surface and aggradation of Q2 with respect to known late Pleistocene environmental changes in southern California due to climate variability. Yellow boxes show the approximate age range of geochronology samples for Q3p and Q2. Note that genesis of the Q3p surface correlates with 50% decrease in precipitation, transition from Pine to Juniper-Oak woodland and a period of stable sea level. Q2 aggradation correlates to aggradation in the San Gabriel Mts., change to drier climate, transition to Chaparral vegetation and rising eustatic sea level.

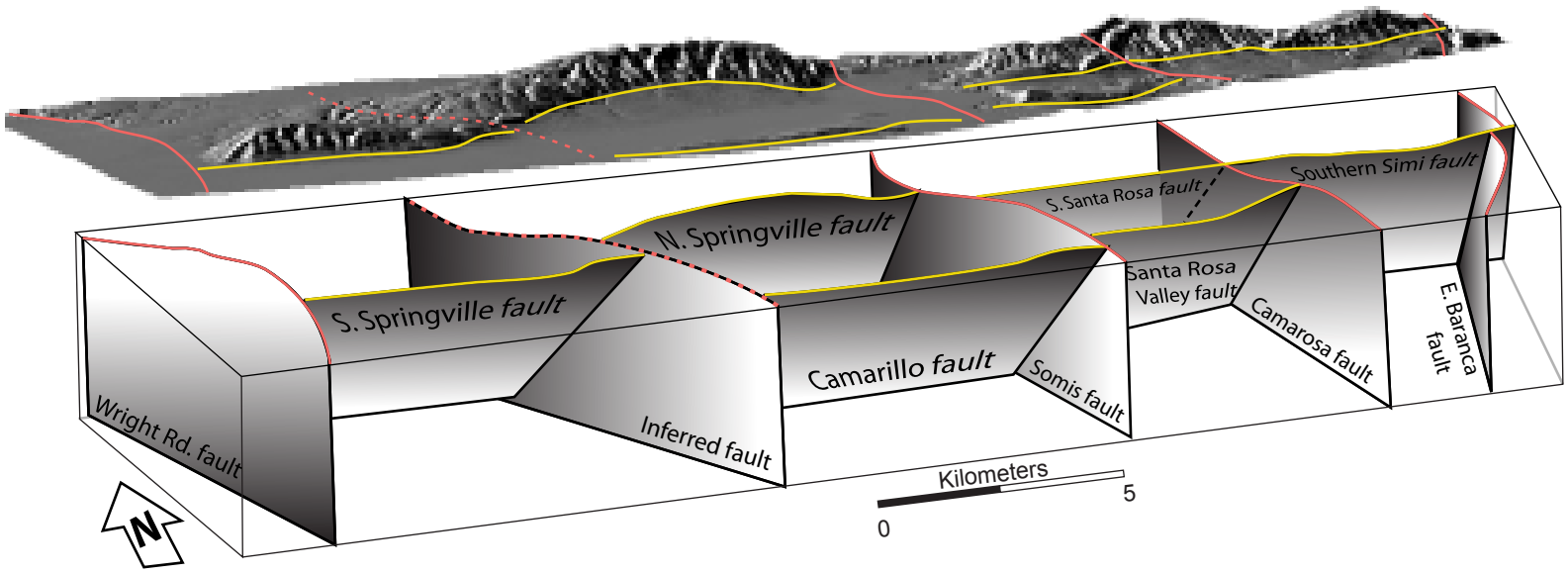

Figure 16.
Three dimensional block model showing our interpretation of the subsurface structure of the important faults in the CFB. Note the change in loci of deformation across the transverse faults (red), with the exception of the southern Simi and Southern Santa Rosa faults, which appear to join and cut across East Baranca and Camarosa faults.

Table 1. Geochronology of the Camarillo fold belt

Sample Number	Age (ka)*	Geomorphic feature	Method	Unit	^{238}U (ppm)	^{232}Th (ppm)	^{40}K (%)	Δ W[α†]	DR_{Cosm} (Gy/ka)[§]	Total DR (Gy/ka)	De (Gy)[#]	Location[**]
1	> 45[††]	Upland Road Anticline	OSL	Q4	1.18±0.05	4.29±0.17	2.57±0.11	1.15±0.07	0.16±0.01	2.85±0.21	Min. 129	318247 3791107
2	> 45[††]	Camarillo Hills Anticline	OSL	Q4	1.48±0.11	8.25±0.41	2.52±0.10	1.15±0.07	0.17±0.01	3.42±0.25	Min. 129	310474 3792386
3	> 45[††]	Springville Anticline	OSL	Q4	1.49±0.03	4.89±0.04	2.69±0.23	1.15±0.07	0.14±0.01	2.96±0.26	Min. 136.56	306417 3789099
4	35 ± 10	Springville Anticline	OSL	Q4	1.59±0.04	5.14±0.04	2.45±0.21	1.15±0.07	0.14±0.02	2.87±0.24	318.4±10.8	306417 3789099
5	84 ± 7	Springville Anticline	IRSL	Q4	2.71±0.03	7.82±0.04	2.54±0.23	1.15±0.07	0.14±0.01	3.79±0.28	98.55±27.31	306417 3789099
6	78 ± 6	Camarillo Hills Anticline	IRSL	Q4	4.91±0.05	10.81±0.05	2.22±0.20	1.15±0.07	0.17±0.01	4.19±0.29	326.7± 7.0	310474 3792386
7	86 ± 6	Upland Road Anticline	IRSL	Q4	4.75±0.05	7.32±0.03	2.63±0.16	1.15±0.07	0.15±0.01	4.27±0.28	365.1±10.3	318247 3791107
8	27 ± 4	Strath terrace	OSL	Q3s	1.33±0.03	4.13±0.03	2.56±0.19	1.15±0.07	0.20±0.01	2.87±0.28	78.18±9.99	317585 3793613
9	25 ± 2	Strath terrace	OSL	Q3s	2.71±0.05	7.93±0.05	2.39±0.16	1.15±0.07	0.17±0.01	3.25±0.25	80.23±2.09	332000 3795598
10	23 ± 1[§§]	Strath terrace	RC	Q3s	—	—	—	—	—	—	—	Approximately located on Figure 4
11	26 ± 4	Camarillo Anticline	OSL	Q3a	1.48±0.03	5.91±0.05	2.77±0.18	1.15±0.07	0.15±0.01	3.17±0.25	81.94±11.38	310551 3787785
12	20 ± 3	Camarillo Anticline	OSL	Q3a	1.40±0.03	4.27±0.03	2.99±0.17	1.15±0.07	0.15±0.01	3.25±0.25	65.26±7.95	310551 3787785
13	32 ± 6	Camarillo Anticline	OSL	Q3a	1.41±0.03	4.29±0.03	2.63±0.17	1.15±0.07	0.17±0.01	2.96±0.23	95.59±17.07	310559 3787797
14	28 ± 2	Camarillo Anticline	OSL	Q3a	2.06±0.04	6.61±0.05	2.81±0.19	1.15±0.07	0.14±0.01	3.36±0.26	93.32±2.13	310895 3787709
15	18 ± 2	Camarillo Anticline	OSL	Q3a	2.21±0.04	8.77±0.07	2.22±0.19	1.15±0.07	0.11±0.01	2.99±0.24	54.62±2.85	310911 3787679
16	29 ± 8	Camarillo Anticline	OSL	Qc2	2.10±0.04	7.96±0.06	2.43±0.18	1.15±0.07	0.14±0.01	3.12±0.25	91.04±19.71	310895 3787709
17	30 ± 3	Camarillo Anticline	OSL	Qc2	2.13±0.04	9.39±0.08	2.34±0.19	1.15±0.07	0.14±0.01	3.14±0.25	93.32±4.73	310895 3787709
18	41 ± 4	Camarillo Anticline	OSL	Qc1	2.18±0.04	9.41±0.07	2.10±0.18	1.15±0.07	0.14±0.01	2.95±0.24	120.06±5.96	310914 3787679
19	5 ± 1		OSL	Q2	3.89±0.07	12.40±0.10	2.25±0.20	1.15±0.07	0.17±0.01	3.64±0.28	17.41±1.07	311397 3797343
20	13 ± 1		OSL	Q2	3.15±0.06	11.80±0.0	2.04±0.17	1.15±0.07	0.15±0.01	3.25±0.25	40.97±3.2	319672 3798155
21	850-780[##]	North of the CFB	Biostrat	Qs	—	—	—	—	—	—	—	Approximately located on Figure 2
22	450-700[***]	Upland Road Anticline	AAR	Qtlp	—	—	—	—	—	—	—	Approximately located on Figure 2

*Errors given, which include: a) for OSL, uncertainties in the equivalent doses, dose rates and age determinations are expressed at the 1σ confidence level. b) for radiocarbon, error is expressed at 2σ confidence interval.

†Estimated water content given in the Δ-notation (weight wet sample / weight dry sample).

§Cosmic doses and attenuation with depth were calculated using the methods of Prescott and Stephans (1982) and Prescott and Hutton (1994).

#Average equivalent dose (D_E) and error ($1\sigma_{n-1}$ of the DE), incorporating the error from beta source estimated at about ±5%.

**Locations are given in Universal Transverse Mercator (UTM) coordinates system zone 11, using World Geodetic System 1984 (WGS84) datum.

††All aliquots in saturation. Only a minmum age can be assessed.

§§Radiocarbon age from Blake (1991)

##Biostratigraphic age from the Moorpark Mammoth site (Wagner et al., 2007). Fossil site is wihtin the Saugus Formation in the uplifted hangingwall of the Oak Ridge fault north of the CFB.

***Amino acid racemization age of shell samples collected from the Las Posas Sand (Boales, 1991).

Table 2. Fault characteristics and potential maximum moment magnitude estimates

Fault	Anticline(s)	Length[a] (km)	Activity[b]	Max (M_w)[c]	Max (M_w)[d]	Max (M_w)[e]
Simi Fault System						
NE. Simi segment	Las Posas	3.8	PA	5.8	5.8	6.0
NW. Simi segment	Las Posas	3.5	PA	5.7	5.7	6.0
Southern Simi	Las Posas	24	A	6.5	6.7	6.7
Santa Rosa Fault System						
N. Santa Rosa	Upland Ridge	3.8	AA	5.8	5.8	6.0
C. Santa Rosa	Upland Ridge	2.8	AA	5.7	5.6	5.9
S. Santa Rosa	Upland Ridge	4.4	AA	5.8	5.8	6.1
Santa Rosa Valley	Valley	4.8	AA	5.9	5.9	6.1
Springville Fault System						
N. Springville A (25°)	Camarillo Hills	6	AA	5.9	6.0	6.2
N. Springville B	Camarillo Hills	6	AA	5.9	6.0	6.2
S. Springville	Springville	3.5	A	5.7	5.7	6.0
Camarillo Fault System						
Camarillo	Camarillo	5.5	AA	5.9	5.9	6.1
North Striking Transverse Tear Faults						
E. Baranca Rd.		>3	inactive	Coseismic[f]	Coseismic[f]	Coseismic[f]
Camarosa		>4.5	PA	Coseismic[f]	Coseismic[f]	Coseismic[f]
Somis		6.5	PA	Coseismic[f]	Coseismic[f]	Coseismic[f]
Wright Rd.		>7.5	AA	Coseismic[f]	Coseismic[f]	Coseismic[f]

[a]Fault length is assumed to be the surface rupture length and may be slightly different than map length

[b]A = Active: demonstrated Holocene (11,500 B.P.); AA = Apparently Active: very young (Probably Holocene) togographic expression of activity; PA = Potentially Active: Active in Pleistocene (last 1.8 m.y.)

[c]Moment Magnitude estimate based on rupture area with and assumed fault depth of 12 km, using the regression of global datasets of Wells and Coppersmith (1994)

[d]Moment Magnitude estimate if the entire length ruptured the surface, using regression analysis of global dataset of Wells and Coppersmith (1994)

[e]Moment Magnitude estimation based on rupture area with and assumed fault depth of 12 km, using the regression of southern California datasets of Dolan et al. (1995)

[f]Not interpreted to be a seismic source. Slip along the fault likely occurs coseismically with slip on adjacent reverse faults.

Table 3. Estimates of vertical offset and rates of faulting within the Camarillo Fold Belt.

Fault	Anticline(s)	Minimum vertical uplift (m)	Preferred vertical uplift (m)	Age range of offset strata (ka)	Minimum vertical uplift rate (mm/yr)
Simi Fault System					
NE. Simi segment	Las Posas	0	N/A	<85[a]	unknown
NW. Simi segment	Las Posas	0	N/A	<85[a]	unknown
Southern Simi	Las Posas	210	230	<85[a]	1.5[c]
Santa Rosa Fault System					
N. Santa Rosa	Upland Rd.	N/A	N/A	<85[a]	unknown
C. Santa Rosa	Upland Rd.	N/A	N/A	<85[a]	unknown
S. Santa Rosa	Upland Rd.	70	125	<85[a]	0.6[c]
Santa Rosa Valley	Q3p surface	35	35	<85[a]	1.5
Springville Fault System					
N. Springville A (25°)	Hills	150	210	<85[a]	unknown
N. Springville B	Hills	150	210	<85[a]	1.4[c]
S. Springville	Springville	75	75	<85[a]	1.6
Camarillo Fault System					
Camarillo	Camarillo	25	40	21-30[b]	1.5
North Striking Transverse Tear Faults					
E. Baranca Rd.		80	>80	>85[a]	unknown
Camarosa		40	70	<85[a]	0.5[c]
Somis		N/A	N/A	N/A	unknown
Wright Rd.		20	N/A	5-12[c]	1.6

[a]Age estimate based IRSL dates of Q4 strata.

[b]Age estimate based on BLSL dates of Q3a strata.

[c]Age estimate based on BLSL of Q2 strata (DeVecchio, 2009).

[c]Vertical uplift rate based on best estimate of the age of Pleistocene terrestrial strata deformed along the fault.